Soft and nonsoft structural transitions in disordered nematic networks

Nariya Uchida*

Department of Physics, Kyoto University, Kyoto 606, Japan

(Received 31 March 2000)

Properties of disordered nematic elastomers and gels are theoretically investigated with emphasis on the roles of nonlocal elastic interactions and crosslinking conditions. Networks originally crosslinked in the isotropic phase lose their long-range orientational order by the action of quenched random stresses, which we incorporate into the affine-deformation model of nematic rubber elasticity. We present a detailed picture of mechanical quasi-Goldstone modes, which accounts for an almost completely soft polydomain-monodomain (PM) transition under strain as well as a ''four-leaf clover'' pattern in depolarized light scattering intensity. Dynamical relaxation of the domain structure is numerically studied using a simple model. The peak wave number of the structure factor obeys a power-law-type slow kinetics and goes to zero in true mechanical equilibrium. The effect of quenched disorder on director fluctuation in the monodomain state is analyzed. The random frozen contribution to the fluctuation amplitude dominates the thermal one, at long wavelengths and near the PM transition threshold. We also study networks obtained by crosslinking polydomain nematic polymer melts. The memory of the initial director configuration acts as correlated and strong quenched disorder, which renders the PM transition nonsoft. The spatial distribution of the elastic free energy is strongly dehomogenized by external strain, in contrast to the case of isotropically crosslinked networks.

PACS number(s): 61.30.Cz, 61.41.+e, 64.70.Md

I. INTRODUCTION

Elastomers and gels are intrinsically disordered solids that retain the memory of their initial states. The nonequilibrium processes of their fabrication create frozen heterogeneities in the network structure, which range in size from mesoscopic to macroscopic scales [1,2]. The presence of the quenched disorder comes to the fore when we introduce some soft order in the system. For instance, density fluctuations of swollen gels near the critical point are strongly enhanced by the heterogeneities. Under stretching, they produce the so-called ''abnormal butterfly'' pattern in small-angle neutron-scattering intensity [3–6]. It illustrates how the elasticity of gels gives rise to a non-trivial effect unexpected in other random systems. Here we address another example of soft order in disordered elastic networks.

Nematic liquid-crystalline elastomers and gels constitute a unique class of solids characterized by a coupling between the orientational and translational degrees of freedom. Physical consequences of the strain-orientation coupling have been the subject of a considerable amount of studies, both theoretical and experimental. We may summarize some important theoretical advances as follows: (i) De Gennes [7] showed that a spontaneous elongation along the director is induced by the isotropic-nematic (IN) transition; (ii) a molecular model of nematic networks was constructed by Warner *et al.* [8], extending the classical affine-deformation model of rubber elasticity; (iii) uniformly oriented networks possess soft modes of strain and orientation fluctuations that do not accompany any change of rubber-elastic free energy. It was first predicted by Golubović and Lubensky [9] on a phenomenological basis and later extended by the affine-

deformation theory [10,11]. Thus, and in other ways, the behavior of homogeneous and clean nematic networks is now fairly well understood [12].

In practice, however, nematic networks in equilibrium quite often exhibit polydomain director textures, where the orientational correlation length is typically in the micron range. Under external strain, polydomain networks undergo a structural change into a macroscopically aligned monodomain state, where the director lies along the extensional direction. This change, called the polydomain-monodomain (PM) transition, is characterized by a highly nonlinear mechanical response [13–19]. The strain-stress curve shows a small slope in the partially aligned (polydomain) state. Depending on the material and the method of synthesis, the slope is sometimes vanishingly small while it is sizable in other cases. The macroscopic stress as a function of strain shows a steep rise as the system turns into the monodomain state.

There have been a few theoretical attempts to describe polydomain networks and their mechanical responses. ten Bosch and Varichon [20] set up the first model, in which they attributed the origin of the equilibrium texture to a random anchoring field exerted by network crosslinks. An interesting analogy with random anisotropy magnets [21] was pursued by Fridrikh and Terentjev [22]. They proposed a mapping to the random-field XY model under an external magnetic field, from which analysis they predicted a discontinuous stress-orientation curve.

Nonetheless, the role of strain-orientation coupling in polydomain networks is still far from clear. There are two aspects to be considered. First, the previous theories assume only local interactions between domains, for instance by arguing that the elastic free energy localizes in domain walls under strain [22]. In general, however, inhomogeneities in an elastic material cause nonlocal or long-range interactions

---

*Electronic address: uchida@ton.scphys.kyoto-u.ac.jp

mediated by the strain field. Such elastic interactions control the physics of various systems, e.g., solids with dislocations [23] or surface defects [24,25], phase-separating alloys [26,27], gels undergoing swelling [28,29], and membranes with inclusions [30]. Disordered nematic networks provide another intriguing example, and differ from most of the above materials in having a nonscalar order parameter. Second, the mechanical response should strongly depend on the crosslinking condition. Polydomain elastomers have been obtained by either of the following ways [14,17]: (i) to crosslink a polymer melt in the isotropic phase and then cool it into the nematic phase; (ii) to crosslink a nematic polymer melt containing polydomain textures. These two cases have not been theoretically well distinguished so far. We shall refer to them as the cases of isotropic and anisotropic crosslinkings, respectively.

Recently, we studied the elastic interaction in isotropically crosslinked networks [31], and found an almost completely soft PM transition [32]. The macroscopic stress due to the strain-orientation coupling was shown to be slightly negative and of $O(\alpha^2)$ in the PM transition region, where α is the degree of chain anisotropy. This contrasts with the earlier prediction of a positive stress of $O(\alpha)$ [22]. The elastic interaction also produces a ''four-leaf clover'' pattern in the depolarized light scattering intensity, which resembles the experimental observation by Clarke *et al.* [16,21].

In this paper, we extend previous work [31,32] and provide the details of our picture of the PM transition. Here let us summarize the ideas and results which we have not emphasized in previous work. First, we pursue the idea that random internal stresses destroy the long-range orientational order, which was suggested (but not proven) earlier in a broader context [9]. This will be done by incorporating the notion of frozen heterogeneous strains into the extended affine-deformation theory [8]. We argue that the random internal stresses act as stronger sources of disorder than the random molecular field due to crosslinks [20,21]. We demonstrate the prediction [9] of critical enhancement of orientational fluctuation by frozen heterogeneities, by analysis of director modes in the monodomain state. Second, evolution of domain structure with and without external stretching is numerically simulated by a simplified dynamical model. The ''four-leaf clover'' scattering pattern has four peaks at finite wave numbers, and the peak height is a nonmonotonic function of the macroscopic strain, in qualitative agreement with experiment. We find a slow dynamical relaxation of the structure factor, and show that the peak wave number asymptotically goes to zero in the long-time limit. Third, we study the case of anisotropic crosslinking. In this case, the initial director configuration of a macroscopic polydomain texture is memorized into the network. It provides a source of strong and correlated disorder, resulting in a nonsoft PM transition. The spatial distribution of elastic free energy in anisotropically crosslinked networks is strongly dehomogenized by strain, while that in isotropically crosslinked networks is unchanged during the PM transition.

This paper is organized as follows. In Sec. II, we introduce a random stress model, derive an effective free energy, and discuss the mechanism of the soft mechanical response. Section III describes a numerical simulation of the polydomain state and the PM transition. In Sec. IV, we analyze the
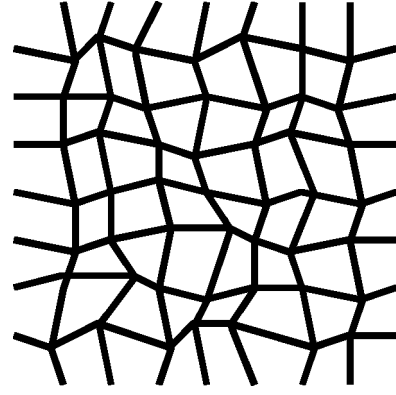

FIG. 1. Schematic illustration of disordered network structure. When the nematic order is introduced, the director is preferentially oriented along the extensional axes of frozen network strains.

effect of random stresses on director fluctuations in the monodomain state. We study networks prepared in the nematic phase in Sec. V. In Sec. VI, we summarize the results in comparison to existing experiments, and conclude with a proposal of future directions.

II. MODEL AND ANALYSIS

A. Random stresses in isotropic networks

It has been known for a long time [1,33] that the network structure of gels is often heterogeneous on many length scales, which are considerably larger than the mesh size (see Fig. 1). In the swollen state, these imperfections manifest themselves as density inhomogeneity and are observed through the so-called butterfly pattern in neutron-scattering intensity or as speckles in light scattering experiment [2,6]. Although less frequently discussed in the literature, it is natural to expect that elastomers, often fabricated by drying gels, also contain the memory of heterogeneous network formation. The frozen heterogeneities reflect the nonequilibrium nature of the crosslinking processes, and produce random internal stresses in the material. While the roles of random stresses in gels and other amorphous solids have been discussed from a phenomenological point of view [9,34], much remains to be done to understand them on the basis of a molecular theory [35]. In this subsection, we recapitulate the notion of random stresses using the classical affine-deformation theory of isotropic rubber networks [36], in order to prepare for modeling disordered nematic networks in the next subsection.

The basic object in the affine-deformation theory is the probability distribution of the chain's end-to-end vector $\boldsymbol{\rho}$. The distribution function at thermal equilibrium is isotropic and Gaussian, and is given by

$$P_{\mathrm{eq}}(\boldsymbol{\rho}) = \mathcal{N}^{-1}\exp\left(-\frac{d}{2\Omega}\rho^2\right), \qquad (1)$$

where $\Omega = \langle \rho^2 \rangle_{\mathrm{eq}}$ is a constant, d is the spatial dimension, and $\mathcal{N} = \int d\boldsymbol{\rho}\, P_{\mathrm{eq}}(\boldsymbol{\rho})$ is the normalization factor. The macroscopic deformation of the network is described by the Cauchy deformation tensor,

$$\Lambda_{ij} = \frac{\partial r_i}{\partial r_{0j}}, \qquad (2)$$

where $\mathbf{r}$ and $\mathbf{r}_0$ are the positions of material points at observation and at the moment of crosslinking, respectively. The basic assumption of the theory is that each chain's end-to-end vector affinely changes as $\boldsymbol{\rho} \rightarrow \boldsymbol{\Lambda} \cdot \boldsymbol{\rho}$ in response to the macroscopic deformation. The free energy per chain is given by [36]

$$f_{\text{chain}} = -k_B T \int d\boldsymbol{\rho} \ P_0(\boldsymbol{\rho}) \ln P_{eq}(\boldsymbol{\Lambda} \cdot \boldsymbol{\rho}), \qquad (3)$$

where $P_0(\boldsymbol{\rho})$ is the probability distribution function at the moment of crosslinking, which is not necessarily identical to the equilibrium distribution. We assume that the chains are distorted before crosslinking, and denote the deviation from the equilibrium conformation by a tensor $\mathbf{R}$, defined by

$$\langle \boldsymbol{\rho}\boldsymbol{\rho} \rangle_0 = \Omega(\mathbf{I} + \mathbf{R}), \qquad (4)$$

where $\mathbf{I}$ is the unit tensor. If the deviation is not very large and the chains are not stretched out, we may still approximate P_0 to be Gaussian, and set

$$P_0(\boldsymbol{\rho}) = \mathcal{N}_0^{-1} \exp\left[\frac{d}{2\Omega} \boldsymbol{\rho} \cdot (\mathbf{I} + \mathbf{R})^{-1} \cdot \boldsymbol{\rho} \right]. \qquad (5)$$

Substituting Eqs. (1) and (5) into Eq. (3), we have

$$f_{\text{chain}} = \frac{k_B T}{2} [\text{Tr } \mathbf{G} + \mathbf{R} : \mathbf{G} + \ln \det(\mathbf{I} + \mathbf{R})], \qquad (6)$$

where $G_{ij} = \Lambda_{ki} \Lambda_{kj}$ is the metric tensor of deformation. Equation (6) is not new and essentially contained in the classical theory of Flory [38]. Taking the spatial heterogeneity of R into account and neglecting terms independent of $\boldsymbol{\Lambda}$, the total elastic free energy is written as

$$F_{\text{el}} = \frac{k_B T \nu_0}{2} \int d\mathbf{r}_0 (\text{Tr } \mathbf{G} + \mathbf{R} : \mathbf{G}), \qquad (7)$$

where ν_0 is the number density of subchains. Inhomogeneous contribution of the form $\mathbf{R} : \mathbf{G}$ can be also derived from Cauchy's theory of solids bound by a central force [34,37]. We shall call R_{ij} the quenched random stress [9], although it is more directly related to quenched random *strain* in the present model. For simplicity, we assume that the frozen heterogeneities have a single characteristic size ξ_R, which is substantially larger than the mesh size. After a coarse-graining on the scale ξ_R, we can regard R_{ij} as a spatially uncorrelated Gaussian random variable satisfying

$$\langle R_{ij}(\mathbf{r}_0) \rangle = 0, \qquad (8)$$

$$\langle R_{ij}(\mathbf{r}_0) R_{kl}(\mathbf{r}_0') \rangle = \xi_R^d \delta(\mathbf{r}_0 - \mathbf{r}_0')$$
$$\times \left[\beta^2 \left(\delta_{ik}\delta_{jl} + \delta_{il}\delta_{jk} - \frac{2}{d} \delta_{ij}\delta_{kl} \right) \right.$$
$$\left. + \beta'^2 \delta_{ij}\delta_{kl} \right]. \qquad (9)$$

The dimensionless constants β and β' represent the magnitudes of shear and dilatational quenched strains, respectively.

B. Random stresses in nematic networks

Next we consider nematic elastomers and gels. Warner *et al.* [8] constructed an affine-deformation theory of nematic networks by generalizing the classical theory. Their basic observation is that nematic chains with low backbone rigidity are well characterized by an anisotropic Gaussian conformation, elongated along the director. The equilibrium distribution of the end-to-end vector can be written in the form

$$P_{\text{eq}}(\boldsymbol{\rho}) = \mathcal{N}'^{-1} \exp\left[-\frac{d}{2\Omega'} \boldsymbol{\rho} \cdot (\mathbf{I} - \alpha\mathbf{Q}) \cdot \boldsymbol{\rho} \right], \qquad (10)$$

where α is the degree of chain anisotropy and

$$Q_{ij} = Q_0 \left(\delta_{ij} - \frac{1}{d} n_i n_j \right) \qquad (11)$$

is the orientational order parameter with $\mathbf{n}$ being the director. We consider a system deep in the nematic phase and set $Q_0 = 1$; the state of orientation is completely specified by the director. The coupling constant α is expressed in terms of the parameters used in [12] as

$$\alpha = \frac{\ell_\parallel - \ell_\perp}{(1 - 1/d)\ell_\parallel + (1/d)\ell_\perp}. \qquad (12)$$

Note that α does not exceed $d/(d-1)$, the value attained in the anisotropic limit $\ell_\parallel / \ell_\perp \rightarrow \infty$. An advantage of the affine-deformation model is that it can describe arbitrary crosslinking conditions; the networks can be fabricated either in the isotropic or the nematic phase. First we consider networks originally crosslinked in the isotropic phase, and we shall treat the case of anisotropic crosslinking in Sec. V. The random stresses are now readily incorporated into the original model. For the case of isotropic crosslinking, the initial chain conformation can be described by Eq. (5), with Eqs. (8) and (9). Substituting Eqs. (5) and (10) into Eq. (3), and dropping terms independent of $\boldsymbol{\Lambda}$ and/or $\mathbf{Q}$, we arrive at the elastic free energy,

$$F_{\text{el}} = \frac{\mu}{2} \int d\mathbf{r} \ \text{Tr}[(\mathbf{I} + \mathbf{R}) \cdot \boldsymbol{\Lambda}^T \cdot (\mathbf{I} - \alpha\mathbf{Q}) \cdot \boldsymbol{\Lambda} - \mathbf{I}] \qquad (13)$$

with $\mu = k_B T \nu_0 (\Omega/\Omega')$. Here we subtracted a constant so that F_{el} vanishes when $\boldsymbol{\Lambda} = \mathbf{I}$ and $\alpha = \beta = 0$. We also replaced $\int d\mathbf{r}_0$ with $\int d\mathbf{r}$, assuming an incompressible network and imposing the local constraint,
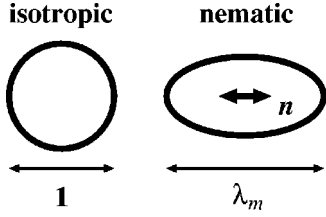
isotropic   nematic

FIG. 2. Spontaneous macroscopic elongation of an ideal (clean) nematic gel, induced by the IN transition.

$$\det \mathbf{\Lambda} = 1. \tag{14}$$

We decompose the elastic free energy into proper and disorder contributions as $F_{el} = F_{el}^P + F_{el}^D$, where, by definition, the former is given by formally setting $\mathbf{R} = 0$ in the right-hand side of Eq. (13), and

$$F_{el}^D = \frac{\mu}{2} \int d\mathbf{r} \; \mathrm{Tr}[\mathbf{R} \cdot \mathbf{\Lambda}^T \cdot (\mathbf{I} - \alpha \mathbf{Q}) \cdot \mathbf{\Lambda}]. \tag{15}$$

The total free energy of the system is written as $F = F_{el} + F_F$, where F_F is the Frank free energy, for which we use the so-called one-constant approximation [39],

$$F_F = \frac{K}{2} \int d\mathbf{r} (\nabla \mathbf{n})^2. \tag{16}$$

We assume that the average deformation $\bar{\Lambda}_{ij}$ is a uniaxial strain along the x axis, parametrized by the elongation ratio λ, as

$$\bar{\mathbf{\Lambda}} = \lambda \mathbf{e}_x \mathbf{e}_x + \lambda^{-1/(d-1)} (\mathbf{I} - \mathbf{e}_x \mathbf{e}_x). \tag{17}$$

The internal displacement is defined as the deviation from the average deformation,

$$\mathbf{u} = \mathbf{r} - \bar{\mathbf{\Lambda}} \cdot \mathbf{r}_0, \tag{18}$$

with which the deformation tensor is expressed as

$$\Lambda_{ij} = \bar{\Lambda}_{kj} (\delta_{ki} + \partial_k u_i) \tag{19}$$

(here and hereafter, we imply summation over repeated indices i, j, k, l, and m).

In the absence of quenched disorder, the elastic free energy is minimized at $\lambda = \lambda_m$ and $\mathbf{u} = 0$, where

$$\lambda_m = \left[\frac{1 + (1/d)\alpha}{1 - (1 - 1/d)\alpha} \right]^{(d-1)/2d} \tag{20}$$

is the ratio of the spontaneous elongation induced by the isotropic-nematic transition [7,12] (see Fig. 2). However, if the random stresses are strong enough, the long-range orientational order is destroyed and the ground state of the system is shifted to a polydomain state with $\lambda = 1$, as we shall see. Hereafter and throughout the paper, we regard λ as an externally controlled parameter.

C. Effective free energy

In this subsection, we derive the effective free energy in the mechanical equilibrium state under the constraint $\lambda = 1$, and discuss its physical consequences. Substituting Eqs. (17), (18) and (19) into Eq. (13), expanding it with respect to $\nabla \mathbf{u}$, and retaining a bilinear form in $\nabla \mathbf{u}$, $\mathbf{R}$, and $\mathbf{Q}$, we have

$$F_{el}|_{\lambda=1} = \frac{\mu}{2} \int d\mathbf{r} [(\partial_i u_j)^2 + 2(R_{ij} - \alpha Q_{ij}) \partial_i u_j - \alpha R_{ij} Q_{ij}]. \tag{21}$$

From this we eliminate the displacement field using the mechanical equilibrium condition,

$$\frac{\delta F_{el}}{\delta \mathbf{u}} = 0, \tag{22}$$

and the incompressibility condition (23), which to the lowest order in $\nabla \mathbf{u}$ reads

$$\nabla \cdot \mathbf{u} = 0. \tag{23}$$

After a straightforward calculation following the procedure described in [31], we obtain an effective elastic free energy which is correct to the quadratic order in α, β, and β', as

$$\tilde{F}_{el}|_{\lambda=1} = -\frac{\mu}{2} \int_{\mathbf{q}} \{ |(\mathbf{I} - \hat{\mathbf{q}}\hat{\mathbf{q}}) \cdot [\hat{\mathbf{q}} \cdot \mathbf{R}(\mathbf{q}) - \alpha \hat{\mathbf{q}} \cdot \mathbf{Q}(\mathbf{q})]|^2$$
$$+ \alpha \mathbf{R}(\mathbf{q}) : \mathbf{Q}(-\mathbf{q}) \}, \tag{24}$$

where $\hat{\mathbf{q}} = \mathbf{q}/|\mathbf{q}|$ and $\int_{\mathbf{q}} = \int (2\pi)^{-d} d\mathbf{q}$ (the tilde is to put to express the effective nature of the free energy). The proper contribution to the free energy is given by

$$\tilde{F}_{el}^P = -\frac{\mu \alpha^2}{2} \int_{\mathbf{q}} |(\mathbf{I} - \hat{\mathbf{q}}\hat{\mathbf{q}}) \cdot [\hat{\mathbf{q}} \cdot \mathbf{Q}(\mathbf{q})]|^2. \tag{25}$$

In the real space, Eq. (25) is rewritten in the form of a two-body long-range interaction, as

$$\tilde{F}_{el}^P = -\frac{\mu \alpha^2}{2} \int d\mathbf{r} \int d\mathbf{r}' [Q_{ik}(\mathbf{r}) \cdot \partial_i \partial_j G_1(\mathbf{r} - \mathbf{r}') \cdot Q_{jk}(\mathbf{r}')$$
$$+ Q_{ij}(\mathbf{r}) \cdot \partial_i \partial_j \partial_k \partial_l G_2(\mathbf{r} - \mathbf{r}') \cdot Q_{kl}(\mathbf{r}')], \tag{26}$$

where $G_n(\mathbf{r})$ ($n = 1, 2$) are the Green functions defined by

$$(\nabla^2)^n G_n(\mathbf{r}) = -\delta(\mathbf{r}), \tag{27}$$

$$G_n(r \to \infty) = 0. \tag{28}$$

In a similar manner, the disorder part of the free energy is written as

$$\tilde{F}_{el}^D = \mu\alpha \int d\mathbf{r} \int d\mathbf{r}'$$

$$\times \{ R_{ik}(\mathbf{r}) \cdot [-\tfrac{1}{2}\delta_{ij}\delta(\mathbf{r}-\mathbf{r}') + \partial_i\partial_j G_1(\mathbf{r}-\mathbf{r}')] \cdot Q_{jk}(\mathbf{r}')$$

$$+ R_{ij}(\mathbf{r}) \cdot \partial_i\partial_j\partial_k\partial_l G_2(\mathbf{r}-\mathbf{r}') \cdot Q_{kl}(\mathbf{r}')\} + \text{const.} \qquad (29)$$

In a given direction of $\mathbf{R}=\mathbf{r}-\mathbf{r}'$, the kernels $\partial_i\partial_j G_1$ and $\partial_i\partial_j\partial_k\partial_l G_2$ in Eqs. (26) and (29) decay in proportion to R^{-d}.

Let us discuss the physical meaning of the effective free energy. First we consider the disorder part, neglecting the proper elastic interaction for the moment. If we decompose the random stress into the dilatational part $R_{kk}\delta_{ij}/d$ and the shear (traceless) part $R_{ij}-R_{kk}\delta_{ij}/d$, the former makes no contribution to the free energy (21) because of Eq. (23) and the tracelessness of $\mathbf{Q}$. Thus, only the shear portion of the random stresses (whose strength is represented by β) is relevant, at least in the bilinear order. It is intuitively obvious that a mere volume change does not create any preferential director orientation, while anisotropic strain does. As seen from Eq. (29), the random stresses both locally and nonlocally act on the director field. The classical scaling argument by Imry and Ma [40] tells that arbitrary weak random stresses destroy the long-range orientation order in dimensions lower than 4. Although the original Imry-Ma argument assumes an uncorrelated random field, it is easy to see that it also holds in the present case, including the scaling law for the domain size. To see this, it is useful to rewrite the right-hand side of Eq. (29) into the form $\mu\alpha\int d\mathbf{r} \; \mathbf{P}(\mathbf{r}):\mathbf{Q}(\mathbf{r})$, where the effective random field $\mathbf{P}$ has a long-range correlation schematically represented as

$$\langle P_{ij}(\mathbf{r})P_{kl}(\mathbf{r}')\rangle = \xi_R^d [\Pi_{ijkl}\delta(\mathbf{r}-\mathbf{r}') + \Pi'_{ijkl}|\mathbf{r}-\mathbf{r}'|^{-d}], \qquad (30)$$

where Π_{ijkl} depends on the direction of $\mathbf{r}-\mathbf{r}'$ but not on its magnitude. Since both Π_{ijkl} and Π_{ijkl} are dimensionless quantities, there appears no additional characteristic length that affects the Imry-Ma scaling of disorder free energy contained per domain. The domain size or the orientational correlation length, which we denote by ξ, is determined by a balance between the effects of random stresses and Frank elasticity. The effective strength of disorder is expressed by the dimensionless parameter

$$D = \frac{\mu\alpha\beta}{K}\xi_R^2. \qquad (31)$$

According to the Imry-Ma argument, the domain size scales as $\xi/\xi_R \propto D^{2/(d-4)}$ in the weak disorder region $D \ll 1$. For a strong disorder $D \gtrsim 1$, we should have $\xi \sim \xi_R$ and optimization of the director field will reduce the disorder free-energy density roughly by $\mu\alpha\beta$.

Next we turn to the proper elastic interaction. It should play only a secondary role in selecting the domain size ξ because of the invariance of Eq. (25) against a change of scale $\mathbf{q}\to\text{const}\times\mathbf{q}$. However, it creates a characteristic anisotropy in the orientational correlation. We see this first in the two-dimensional (2D) case. In 2D, the orientational configuration is specified by the director's azimuthal angle $\theta = \theta(\mathbf{r})$, as
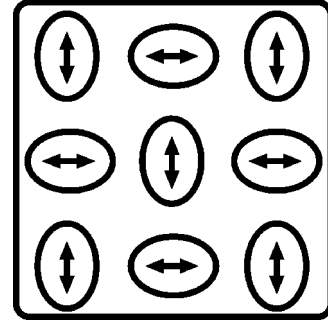

FIG. 3. Preferred local director configuration. Ellipses indicate the anisotropy of local strain. The ''checkered'' structure enables each domain to elongate along the local director, without violating the global constraint $\lambda=1$. Note that the proper elastic interaction does not select the characteristic size of the pattern.

$$\mathbf{n}=(\cos\theta, \sin\theta), \qquad (32)$$

or, equivalently,

$$\mathbf{Q}=\frac{1}{2}\begin{bmatrix} \cos 2\theta & \sin 2\theta \\ \sin 2\theta & -\cos 2\theta \end{bmatrix}. \qquad (33)$$

A straightforward calculation reduces Eq. (26) to

$$\tilde{F}_{el}^P = \frac{\mu\alpha^2}{16\pi}\int d\mathbf{r}\int d\mathbf{r}' \frac{1}{R^2}\cos[2(\theta(\mathbf{r})-\psi) + 2(\theta(\mathbf{r}')-\psi)], \qquad (34)$$

where ψ is the azimuthal angle of $\mathbf{R}=\mathbf{r}-\mathbf{r}' = |\mathbf{R}|(\cos\psi, \sin\psi)$. From the angle dependence of the integrand, we expect that the above free energy is minimized by a ''checkered'' domain configuration as depicted in Fig. 3. Correlation in directions parallel and perpendicular to the local director is suppressed, while those in oblique directions are enhanced. It has the following simple interpretation. Upon the isotropic-nematic transition, each part of the network tends to elongate along the local director. The domain in the center of the figure pushes the top neighbor upward, pulls the left neighbor rightward, and so on. To reduce the mechanical conflict without violating the global constraint $\lambda=1$, the top and left domains are reoriented perpendicular to the central one. This domain reconfiguration enables the IN transition-induced elongation along the local director, despite spatial inhomogeneity.

The same picture holds for orientational correlation in three dimensions. In 3D, Eq. (26) becomes

$$\tilde{F}_{el}^P = \frac{\mu\alpha^2}{16\pi}\int d\mathbf{r}\int d\mathbf{r}' \frac{1}{R^3}\; g(\mathbf{n},\mathbf{n}',\hat{\mathbf{R}}), \qquad (35)$$

$$g(\mathbf{n},\mathbf{n}',\hat{\mathbf{R}}) = -\frac{5}{3} + 4(\mathbf{n}\cdot\mathbf{n}')^2 + (\mathbf{n}\cdot\hat{\mathbf{R}})^2 + (\mathbf{n}'\cdot\hat{\mathbf{R}})^2$$

$$- 18(\mathbf{n}\cdot\mathbf{n}')(\mathbf{n}\cdot\hat{\mathbf{R}})(\mathbf{n}'\cdot\hat{\mathbf{R}}) + 15(\mathbf{n}\cdot\hat{\mathbf{R}})^2(\mathbf{n}'\cdot\hat{\mathbf{R}})^2, \qquad (36)$$

where $\mathbf{n} = \mathbf{n}(\mathbf{r})$, $\mathbf{n}' = \mathbf{n}(\mathbf{r}')$ and $\hat{\mathbf{R}} = \mathbf{R}/|\mathbf{R}|$. Correlation in the direction parallel to the director is suppressed as in the 2D case, which is known by observing that the function

$$g(\mathbf{n}, \mathbf{n}', \mathbf{n}) = -\tfrac{2}{3} + 2(\mathbf{n} \cdot \mathbf{n}')^2 \qquad (37)$$

takes its minimum when $\mathbf{n} \perp \mathbf{n}'$.

The domain reconfiguration due to the proper elastic interaction is suppressed by the Frank elasticity at wavelengths shorter than

$$\xi_c = \sqrt{\frac{K}{\mu \alpha^2}}. \qquad (38)$$

Thus we have three characteristic length scales: ξ, ξ_R, and ξ_c. The observed domain size ξ is typically $1 - 10^1 \mu$m, while we estimate ξ_c to be 10 nm for typical experimental values $K = 10^{-11}$ J/m, $\mu = 10^5$ J/m^3, and $\alpha = 1.0$. There is a substantial gap between ξ and ξ_c, where the proper elastic interaction plays a dominant role. The Frank free-energy density f_F (averaged over space) scales as $f_F \sim f_{el}^P (\xi_c/\xi)^2 \ll f_{el}^P \sim \mu \alpha^2$. The domain size ξ can be cast into a scaling form,

$$\frac{\xi}{\xi_R} = \Xi\left(D, \frac{\xi_c}{\xi_R}\right). \qquad (39)$$

Although Ξ is a highly nontrivial function, it can be numerically obtainable unless D is very small (or unless ξ/ξ_R is very large), as we see in Sec. III. We have a trial estimate $D \sim 1$ if we assume $\beta \sim 0.01$ and $\xi_R \sim 100$ nm in addition to the above values of K, μ, and α. Of course, this estimate of D is quite uncertain because the magnitudes of β and ξ_R should depend on the kinetics of the crosslinking process, quality of the solvent, etc. Our point here is that it is not unreasonable to have a moderately strong disorder in the presence of submicron-scale network heterogeneities, which is considered ubiquitous.

D. Mechanical response

Now we proceed to discuss the mechanical response during the polydomain-monodomain transition. To do so, it is useful to examine again the polydomain state at $\lambda = 1$ and in 2D. The harmonic free energy (25) can be rewritten as [31]

$$\widetilde{F}_{el}^P = -\frac{\mu \alpha^2}{2} \int_{\mathbf{q}} |Q_1(\mathbf{q})|^2, \qquad (40)$$

$$Q_1(\mathbf{q}) = 2\hat{q}_x \hat{q}_y Q_{xx}(\mathbf{q}) - (\hat{q}_x^2 - \hat{q}_y^2) Q_{xy}(\mathbf{q})$$
$$= \sin 2\varphi \ Q_{xx}(\mathbf{q}) - \cos 2\varphi \ Q_{xy}(\mathbf{q}), \qquad (41)$$

where φ is the azimuthal angle of the wave vector, $\mathbf{q} = |\mathbf{q}|(\cos \varphi, \sin \varphi)$. Complementary to $Q_1(\mathbf{q})$ is the variable defined by

$$Q_2(\mathbf{q}) = (\hat{q}_x^2 - \hat{q}_y^2) Q_{xx}(\mathbf{q}) + 2\hat{q}_x \hat{q}_y Q_{xy}(\mathbf{q})$$
$$= \cos 2\varphi Q_{xx}(\mathbf{q}) + \sin 2\varphi Q_{xy}(\mathbf{q}). \qquad (42)$$

Note that $Q_1(\mathbf{q})$ and $Q_2(\mathbf{q})$ constitute a set of normal modes, and satisfy

$$|Q_1(\mathbf{q})|^2 + |Q_2(\mathbf{q})|^2 = |Q_{xx}(\mathbf{q})|^2 + |Q_{xy}(\mathbf{q})|^2, \qquad (43)$$

or

$$\overline{Q_1(\mathbf{r})^2} + \overline{Q_2(\mathbf{r})^2} = \overline{Q_{xx}(\mathbf{r})^2} + \overline{Q_{xy}(\mathbf{r})^2} = \tfrac{1}{4}, \qquad (44)$$

where $Q_a(\mathbf{r})$ ($a = 1,2$) are the inverse Fourier transform of $Q_a(\mathbf{q})$. To reduce the free energy (40), there arises an asymmetry $Q_1(\mathbf{r})^2 > Q_2(\mathbf{r})^2$. In the limit where $\mu \alpha^2$ is much larger than the disorder and Frank contributions to the free-energy density, we expect from Eq. (44) to have

$$\overline{Q_1(\mathbf{r})^2} = \tfrac{1}{4}, \quad \overline{Q_2(\mathbf{r})^2} = 0, \qquad (45)$$

which indeed is numerically confirmed [32]. In this limit, the elastic free-energy density is given by

$$f_{el} = \frac{\mu \alpha^2}{8}, \qquad (46)$$

as seen from Eq. (40). To the second order in α, it is equal to the free energy in the monodomain state with $\lambda = \lambda_m$, as we can easily check by substituting Eq. (20) into Eq. (13) and expanding it with respect to α. Thus we conclude that the elastic free energy change accompanied with the PM transition is of $O(\alpha^3)$, and the macroscopic stress averaged over the region $1 < \lambda < \lambda_m$, or

$$\frac{f_{el}(\lambda = \lambda_m) - f_{el}(\lambda = 1)}{\lambda_m - 1}, \qquad (47)$$

is a quantity of $O(\alpha^2)$.

To see the origin of the soft response, it is useful to look at the local elastic stress tensor, which is given in the harmonic approximation (21) as [41]

$$\sigma_{ij} = \mu(\partial_i u_j + \partial_j u_i - \alpha Q_{ij} + R_{ij}). \qquad (48)$$

Consider its variance $\overline{\sigma_{ij}^2}$. In the absence of random stresses, we have

$$\int d\mathbf{r} \ \sigma_{ij}^2 = 4\mu F_{el} + \mu^2 \alpha^2 \int d\mathbf{r} \ Q_{ij}^2$$
$$= \mu^2 \alpha^2 \int d\mathbf{r}(Q_{ij}^2 - 2Q_1^2) = 2\mu^2 \alpha^2 \int d\mathbf{r} \ Q_2^2, \qquad (49)$$

which vanishes from Eq. (45). [Here we utilized the relation $0 = \det \Lambda - 1 = \nabla \cdot \mathbf{u} + \tfrac{1}{2}(\nabla \cdot \mathbf{u})^2 - \tfrac{1}{2}(\partial_i u_j)(\partial_j u_i) + O((\nabla \mathbf{u})^3)$ to have $(\partial_i u_j)(\partial_j u_i) = O(\alpha^3)$ in the mechanical equilibrium. We neglected this higher-order term in the expansion of

σ_{ij}^2.] This means that each part of the system is stretched along the local director by $1 + \alpha/4 + O(\alpha^2) \sim \lambda_m$ times. This local elongation, realized by the checkered polydomain structure, reduces the free energy close to its absolute minimum.

III. NUMERICAL SIMULATION

To further study the nonlinear mechanical response and the effect of random disorder, we resort to numerical simulation by the continuum model. We utilize two different numerical schemes, one for the polydomain state in mechanical equilibrium at $\lambda = 1$ and another for the PM transition and dynamical effects. A two-dimensional system is assumed for computational advantage. All the simulations below are performed on an $N \times N$ square lattice with $N = 128$ unless otherwise stated. The grid spacing is chosen to be the unit of length. Periodic boundary conditions are imposed on $\mathbf{n}(\mathbf{r})$ and $\mathbf{u}(\mathbf{r})$, while the average strain λ is externally controlled.

A. Polydomain state

First we study the polydomain state in complete mechanical equilibrium and with no average strain ($\lambda = 1$). To this end, we assume the harmonic free energy (21) and solve the linear equations (22) and (23) using the fast Fourier transform. To minimize the free energy, we adapted a variant of the simulated annealing method [42]. The orientational order parameter is evolved according to a Langevin equation,

$$\frac{\partial \mathbf{n}}{\partial t} = \Gamma_n (\mathbf{I} - \mathbf{n}\mathbf{n}) \cdot \left(-\frac{\delta F}{\delta \mathbf{n}} + \boldsymbol{\eta} \right), \qquad (50)$$

where Γ_n is a constant and $\boldsymbol{\eta}$ is a ''thermal'' noise satisfying

$$\langle \boldsymbol{\eta}(\mathbf{r},t) \boldsymbol{\eta}(\mathbf{r}',t') \rangle = \eta_0^2 \, \mathbf{I} \cdot \delta(\mathbf{r} - \mathbf{r}') \delta(t - t') \qquad (51)$$

and Gaussian statistics. The noise strength η_0 is gradually reduced to zero until the end of each run. To be precise, we decrease η_0 to zero at a constant rate in the former half of a run, and set $\eta_0 = 0$ in the latter half. The initial noise strength and the annealing rate are chosen so that two different initial configurations, one with a random and another with a homogeneous director field, lead to indistinguishable results for the macroscopic quantities such as correlation function, average orientation, and free-energy densities. As a standard set of static parameters we choose

$$\mu = 400, \quad \alpha = 0.2, \quad \beta = 0.025, \quad \xi_R = 1, \quad K = 4, \qquad (52)$$

for which $\xi_c = 0.5$ and $D = 0.5$. We integrated Eq. (50) using the Euler scheme with time increment $\Delta t = 1$ per step. A typical run consisted of 5×10^4 time steps. Longer runs did not make an observable difference in the macroscopic quantities.

First we consider the orientational correlation function,

$$G(\mathbf{R}) = \langle Q_{ij}(\mathbf{r}) Q_{ij}(\mathbf{r} + \mathbf{R}) \rangle, \qquad (53)$$

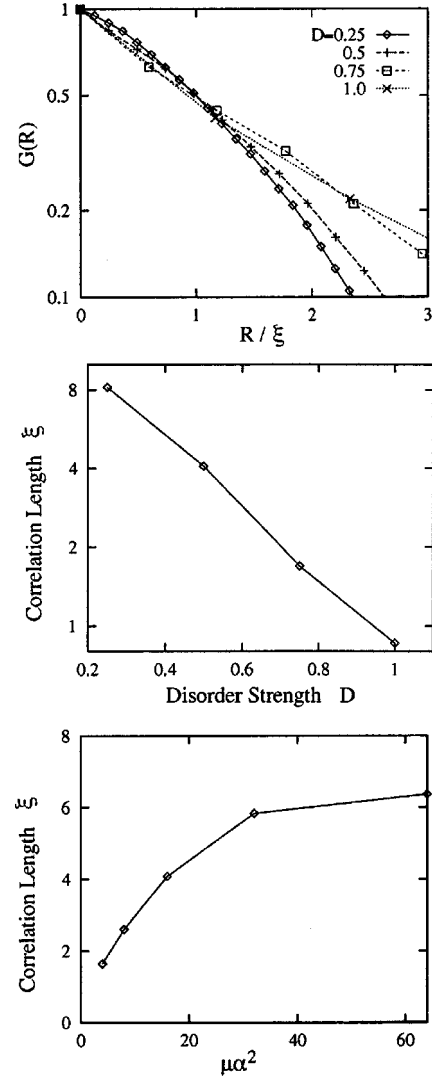which is a function only of distance. We define the correlation length ξ through

FIG. 4. Top: Correlation function $G(R)$ for different disorder strengths. Middle: Correlation length versus disorder strength. In the top and middle plots we fix $\mu\alpha^2 = 16$. Bottom: Correlation length versus strength of elastic interaction. The disorder strength is fixed ($D = 0.5$).

$$\frac{G(\xi)}{G(0)} = \frac{1}{2}. \qquad (54)$$

For each parameter set, we took a statistical average over 20 samples. The data are shown in Fig. 4. The decay of $G(R)$ is nearly exponential for strong disorder and faster than exponential for weak disorder. This qualitative tendency agrees with previous results for the 2D random-field XY model [43–45]. The correlation length is a rapidly decreasing function of the effective disorder strength, D. The dependence is roughly exponential, also in agreement with previous results for the XY model [43,45]. In the same figure we show the dependence of ξ on $\mu\alpha^2$, which is the measure of elastic interaction. Although the dependence is weak, the proper elastic interaction has an effect of increasing the correlation length. This is related to the enhancement of correlation in directions oblique to the local director, depicted in Fig. 3. In order to quantify the director-relative correlation, we define the function
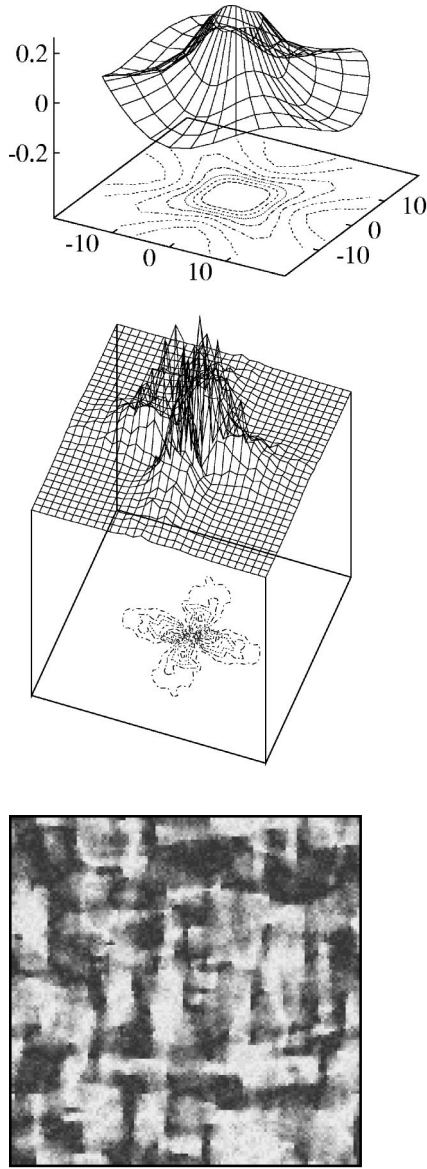
FIG. 5. Top: Director-relative correlation function $H(R)$, plotted in the region $\xi < R < 5\xi$. The unit of length is the grid size Δx. Middle: Depolarized light scattering intensity $\langle |Q_{xy}(\mathbf{q})|^2 \rangle$. Shown is the region $-15 < q_x < 15$ and $-15 < q_y < 15$, where the unit of wave number is $2\pi/(N\Delta x)$. Bottom: Snapshots of the orientational order parameter field $Q_{xy}(\mathbf{r}) = \sin 2\theta$. The value of Q_{xy} is positive in white regions and negative in black regions.

$$H(\mathbf{R}) = \langle Q_{ij}(\mathbf{r}) Q_{ij}[\mathbf{r} + \mathbf{U}(\mathbf{r}) \cdot \mathbf{R}] \rangle, \qquad (55)$$

where $\mathbf{U}(\mathbf{r})$ is a matrix of rotation that maps $\mathbf{n}(\mathbf{r})$ to $\mathbf{e}_x$, or, explicitly,

$$\mathbf{U} = \begin{bmatrix} \cos\theta & -\sin\theta \\ \sin\theta & \cos\theta \end{bmatrix}. \qquad (56)$$

By definition, $H(x,0)$ and $H(0,y)$, respectively, describe the correlation in directions parallel and perpendicular to the local director. The data for the standard parameter are plotted in Fig. 5. We see that the correlation is long-ranged in any specific direction, and the exponential-like decay in Fig. 4

should be considered as a result of mutual cancellation of positive and negative correlation by taking the angular average.

A real-space snapshot of the order-parameter field Q_{xy} is also given in Fig. 5. As the gray scale shows, the contour $Q_{xy} = 0$ preferentially lies in the horizontal (x) and vertical (y) directions. This corresponds to the checkered domain structure in Fig. 3 (note that the gray scale is chosen so that the director is oblique to the horizontal axis in the brightest and darkest regions). More precisely, the checkered pattern is found on many different length scales, which is a natural consequence of the fact that the elastic interaction energy (24) is scale-independent.

An experimentally accessible way to characterize the anisotropic director correlation is the polarized light scattering. In a weakly inhomogeneous state, the depolarized (HV) light scattering intensity is given by

$$I(\mathbf{q}) = \langle |Q_{xy}(\mathbf{q})|^2 \rangle, \qquad (57)$$

except for a $\mathbf{q}$-independent prefactor. According to Ref. [16], the above formula holds even in a highly inhomogeneous state, if one assumes a two-dimensional configuration [see Eq. (2) in the reference]. Our numerical data are shown in Fig. 5. The intensity (57) is expressed in terms of Q_1 and Q_2 as $I(q) = \cos\varphi^2 \langle |Q_1(\mathbf{q})|^2 \rangle + \sin\varphi^2 \langle |Q_2(\mathbf{q})|^2 \rangle$, and the asymmetry $Q_1 > Q_2$ explains the enhanced scattering on q_x- and q_y- axes [31].

Note that the peak is located at a small but finite wave number, contrary to what is expected from the nonconserved nature of the orientational order parameter. In fact, we find it to be a finite-size effect, and the peak wave number shrinks to zero as the system size N is taken to infinity, leaving a singular minimum at the origin. To see this, we have computed the circularly averaged structure factor,

$$S(q) = \int_0^{2\pi} d\varphi |Q_{ij}(\mathbf{q})|^2 \rangle, \qquad (58)$$

for $N = 64$, 128, and 256 systems, and found a peak in the region $(2\pi/N) < q < 2(2\pi/N)$ in every case. The origin of the singular minimum at $q = 0$ is explained as follows. Because of the periodic boundary condition on $\mathbf{u}$, the spatial average $\overline{\nabla \mathbf{u}}$ should completely vanish. This constraint suppresses the formation of the checkered pattern with the check size larger than $N/2$.

B. Polydomain-monodomain transition

Next we study the PM transition using the nonlinear elastic free energy (13). We found that complete minimization of the free energy takes very much computation time. Therefore we decided to take a more empirical approach: with a simple dynamical model, we strained the system continuously, without waiting until complete equilibration. Fortunately, the stress-strain relation thus obtained is equilibrated to a good degree, because of fast relaxation of the rubber-elastic free energy. On the other hand, the domain structure exhibits a slow coarsening, which we study in the absence of external strain.
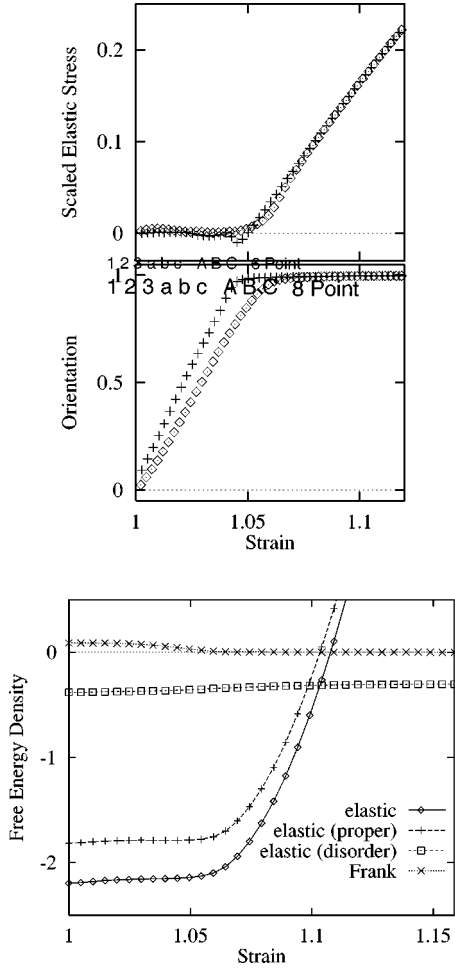
FIG. 7. Strain-stress and strain-orientation curves for $\alpha = 0.2$, 0.4, 0.8, and 1.2 from the left to right. Corresponding values of λ_m are 1.05, 1.11, 1.24, and 1.41, respectively. The parameters $\mu\alpha^2 = 16$ and $D = 0.5$ are common to all cases.

FIG. 6. Top: Strain-stress (λ vs $\mu^{-1}\sigma_{macro}$) and strain-orientation (λ vs S) curves for $\alpha = 0.2$ ($\lambda_m = 1.051$). Diamonds ($\diamond$) and crosses ($+$) are for the loading and unloading processes, respectively. Bottom: Free-energy densities (for the loading process).

Our dynamical model consists of a set of equations that describe the evolution of nonconserved order parameters in the simplest manner, namely,

$$\frac{\partial \mathbf{n}}{\partial t} = -\Gamma_n (\mathbf{I} - \mathbf{nn}) \cdot \frac{\delta F}{\delta \mathbf{n}} \qquad (59)$$

and

$$\frac{\partial \mathbf{u}}{\partial t} = -\Gamma_u \frac{\delta F}{\delta \mathbf{u}}. \qquad (60)$$

Instead of imposing the strict incompressibility condition (23), we penalized the local volume change by adding an artificial potential F_v to the free energy. By taking it in the form $F_v = \frac{1}{2}\int d\mathbf{r}[a_0(\det\mathbf{\Lambda} - 1)^2 + a_1(\det\mathbf{\Lambda} - 1)^4]$ and choosing appropriate values of the constants a_0 and a_1, we kept $\det\mathbf{\Lambda}$ in the region [0.99,1.01] throughout the runs.

We integrated Eqs. (59) and (60) using the Euler scheme with $\Gamma_n = 0.2$, $\Gamma_u = 0.02$, and $\Delta t = 1$. A typical set of static parameters is identical to that given by Eq. (52).

To prepare a polydomain state, we set sitewise random numbers to $\mathbf{Q}$ and $\mathbf{u}$ as the initial condition, and integrated
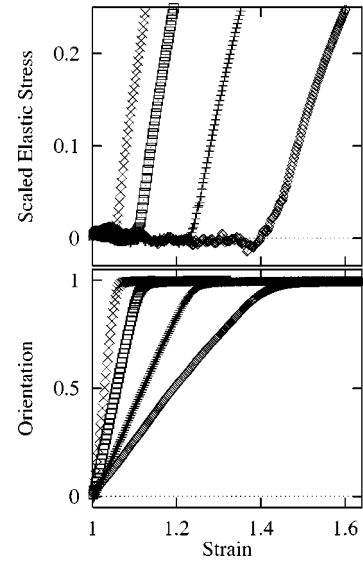
Eqs. (59) and (60) for 5×10^4 time steps with $\lambda = 1$. Then we increased λ at a constant rate $d\lambda/dt = 1 \times 10^{-5}$ to induce the PM transition. To check hysteresis, finally we decreased λ back to unity at the rate $d\lambda/dt = -1 \times 10^{-6}$.

Plotted in Fig. 6 are the scaled macroscopic elastic stress $\mu^{-1}\sigma_{macro} = \mu^{-1}(\partial f_{el}/\partial\lambda)$ and the mean orientation $S = \cos 2\theta = 2Q_{xx}$ as functions of λ. We see from the figure that the elastic stress is vanishingly small and the orientation linearly increases in the polydomain region $1 < \lambda < \lambda_m$ ($= 1.05$). The stress shows a linear rise in the monodomain region $\lambda > \lambda_m$, where the orientation is nearly saturated to the maximum, $S = 1$. While the strain-orientation curve has a small hysteresis, the strain-stress curve is almost completely reversible.

The smallness of the hysteresis manifests an important difference between the present system and random anisotropy magnets under magnetic field. In the latter, the macroscopic orientational order is broken solely by a random field. In contrast, in the present model, the monodomain state is unstable to a strain-mediated director buckling for $\lambda < \lambda_m$,
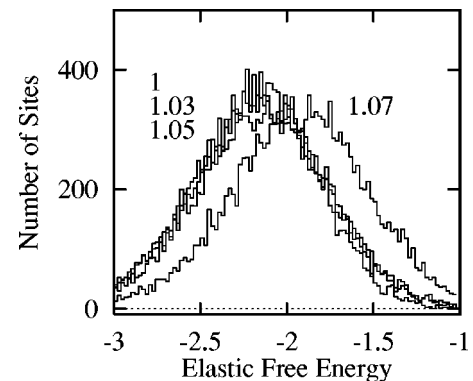

FIG. 8. Histogram of the elastic free energy contained in a site. Distributions for cases $\lambda = 1$, 1.03, 1.05, and 1.07 are shown. The first three are indistinguishable from each other.

λ=1   λ=1.03
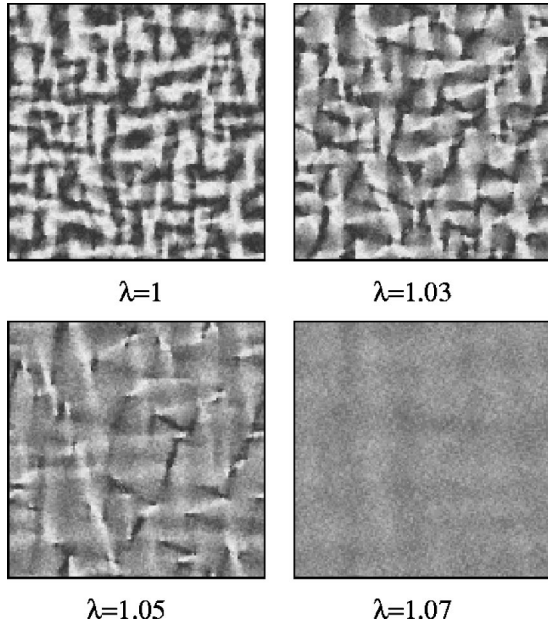
λ=1.05   λ=1.07

FIG. 9. Real-space snapshots of the field $Q_{xy}(\mathbf{r})$.

even when there is no quenched disorder. This instability, which will be discussed in Sec. IV in detail, makes the PM transition almost reversible.

The free-energy densities are also shown in Fig. 6. Both the proper and disorder parts of the rubber-elastic free energy change little in the region $\lambda < \lambda_m$. The latter curve has a slightly positive gradient. The situation is more subtle for the former. Its gradient is slightly positive in the figure, and turns to slightly negative for a smaller disorder strength. However, in the absence of random stresses and at $\lambda = 1$, we had four domains whose sizes are limited by the system size, and the domain boundaries raise the elastic free energy. Because of this finite-size effect, we cannot exactly tell the sign of the proper elastic stress in the macroscopic limit. We cannot exclude the possibility that the macroscopic stress completely vanishes in the limit of weak disorder.

The strain-stress and strain-orientation curves for larger values of α are given in Fig. 7. Each curve shows a sharp crossover around $\lambda = \lambda_m(\alpha)$. The elastic stress in the polydomain region is vanishingly small even for large coupling. For any value of α studied, the changes of the proper and disorder elastic free-energy densities, $|f_{el}^P(\lambda = \lambda_m) - f_{el}^P(\lambda = 1)|$ and $|f_{el}^D(\lambda = \lambda_m) - f_{el}^D(\lambda = 1)|$, were smaller than 0.3%

percent of $\mu \alpha^2$. We find essentially no α-dependence of the macroscopic stress in the polydomain region.

Shown in Fig. 8 is the histogram of the elastic free energy contained in a lattice site. The distribution is fairly sharp and little changed by stretching for $\lambda < \lambda_m$, implying that the free energy is homogeneously minimized in the polydomain state. Real space snapshots of the domain morphology are shown in Fig. 9. Pinned defects are observed just below the threshold $\lambda = \lambda_m$, while we find no defects remaining in the monodomain state.

The depolarized scattering intensity is shown in Fig. 10. It has a minimum at $q = 0$ and develops four peaks at finite wave numbers. As we shall see in the next subsection, the peaks move toward the origin as the true equilibrium is approached and the domains coarsen. Here we concentrate on the effect of stretching. The peak intensity first increases and then decreases as a function of λ. Under stretching along the x axis, the peaks on the q_x axis are more enhanced than those on the q_y axis. The shift of the peak wave number by stretching is very small and difficult to estimate. By our choice of the stretching rate, the PM transition was completed in 5×10^3 time steps, much before a significant coarsening can occur.

C. Slow structural relaxation

Now we turn to dynamical effects. First let us discuss the conditions under which Eqs. (59) and (60) are most reasonable as a model of dynamic evolution, not only as an artificial scheme of functional minimization. First, Eq. (60) means that the velocity $\partial \mathbf{u}/\partial t$ is proportional to the force $-\delta F/\delta \mathbf{u}$. This applies to the motion of a network in a viscous solvent [46], where we have a straightforward analogy to D'arcy's law in porous media. On the other hand, in dry elastomers, there arises a viscous stress due to intranetwork friction, which is proportional to $\nabla(\partial \mathbf{u}/\partial t)$. This is not accounted for in Eq. (60). Thus we consider that the dynamic model is more appropriate to swollen gels than to elastomers. Second, Eqs. (59) and (60) neglect dynamical coupling between the order parameters, i.e., the nondiagonal part of the Onsager coefficient matrix. This does not matter if the dynamics of the orientational order parameter is dynamically "slaved" to the displacement field, which we expect to be the case. In fact, if the constituent polymer of the gel is not rigid, Γ_n^{-1} is of the order of the viscosity of low-molecular-weight fluids, η. On the other hand, the friction between the
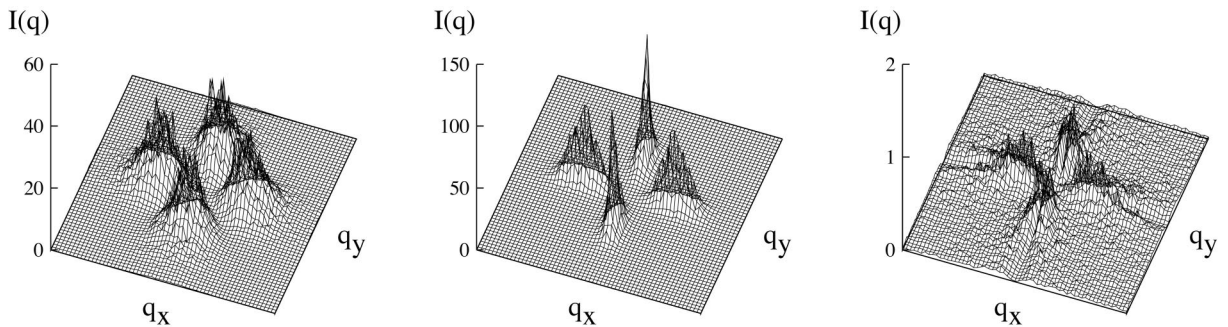

FIG. 10. Depolarized scattering intensity (in arbitrary units) at $\lambda = 1$, 1.03, and 1.05, from the left to right. Statistical average over 20 samples is taken for each case. Shown is the region $-30 < q_x < 30$ and $-30 < q_y < 30$. Note the difference in intensity.
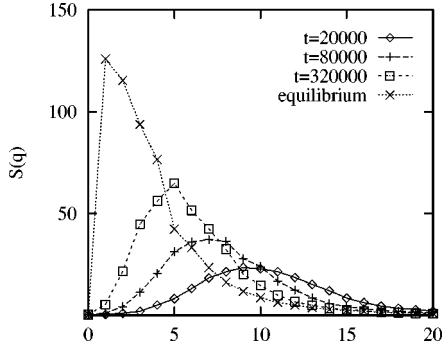
FIG. 11. Circularly averaged structure factor $S(q)$ (in arbitrary unit) at $t=2\times10^4$, 8×10^4, and 32×10^4 steps and in mechanical equilibrium. Statistical average over 20 samples is taken.

network and solvent renders Γ_u^{-1} to be of the order of η/l^2, where l is the mesh size of the network [29,47]. Thus, the characteristic relaxation time of the strain at the scale of domain size is $\sim(\xi/l)^2(\gg1)$ times larger than that of $\mathbf{Q}$.

Evolution of the structure factor $S(q)$ [as defined by Eq. (58)] is shown in Fig. 11. The peak wave number decreases and the peak intensity increases as a function of time. Also shown in the figure is the structure factor at complete mechanical equilibrium, which is obtained by the numerical scheme used in Sec. III A. The correlation length ξ and the inverse of the peak wave number q_0 are plotted in the middle of Fig. 12. In the time region $1\times10^3<t<3\times10^5$, the former is well fitted by a power law $\xi(t)\propto t^\epsilon$ with $\epsilon=0.23\pm0.02$, and the latter grows almost in parallel to the former.

The Frank and rubber-elastic free energies are plotted as functions of time in Fig. 12. While the elastic free energy changes little after an early stage of around $t=10^3$ time steps, the Frank energy density f_F shows a slow and continuous decrease, which is approximately described by a power law $f_F\propto t^{-\epsilon'}$ in the region $1\times10^3<t<3\times10^5$, with $\epsilon'=0.22\pm0.03$.

Presently we have no explanation for the good fits of $\xi(t)$ and $f_F(t)$ by power laws. We point out that the values of ϵ and ϵ' are much smaller than the corresponding exponents for the 2D nonconserved XY model without quenched disorder, which equal 0.5 and 1.0 from a simple scaling argument [48]. The naive scaling relation $\epsilon'=2\epsilon$ is also broken here, which is not at all surprising if we consider the presence of quenched disorder [49]. We should also stress that the final equilibrium values of ξ and f_F are finite. Preliminary study by a longer run without statistics finds a crossover from the

power-law-type kinetics to a slower one at $t\sim1\times10^6$ steps.

The above results show that the relaxation process can be decomposed into three characteristic stages. (i) The quench into the nematic phase from the isotropic phase produces microscopic textures, which coarsen to reduce both the rubber-elastic and Frank free energies. After the characteristic domain size reaches ξ_c, anisotropic domain reconfiguration on this scale follows. The rubber-elastic free energy is almost completely minimized at this early stage, because of the scale independence of the proper elastic interaction (24). (ii) The ''checkered'' domain structure further coarsens to reduce the Frank free energy. The domain size ξ and the peak wavelength $2\pi/q_0$ grow in parallel to each other. (iii) The domain size converges to a finite equilibrium value, while the anisotropic domain reconfiguration proceeds on larger scales $[\lim_{t\to\infty}q_0(t)=0]$.

IV. FLUCTUATION IN THE MONODOMAIN STATE

A. Critical enhancement of soft fluctuation by disorder—Golubović-Lubensky prediction

Recall that, if there is no quenched disorder, the ground state of the system is the macroscopically elongated state with $\lambda=\lambda_m$ and $\mathbf{u}=0$. In this state, there are so-called soft modes of director fluctuation, which do not accompany any change in the rubber-elastic free energy [9–11]. The presence of the soft modes implies that a homogeneous director configuration becomes unstable for $\lambda<\lambda_m$; when we compress the gel along the optical axis, the director ''buckles'' to partially cancel the rise of elastic free energy by compression. The result of the preceding section means that this instability is almost completely soft even for large deformations. In this section, we look at the monodomain region $\lambda\geq\lambda_m$ and analyze the director fluctuation modes in a harmonic level. In a general point of view, our analysis gives a specific demonstration of the prediction by Golubović and Lubensky [9] on a class of elastic systems that undergo a spontaneous shear deformation (''anisotropic glasses'' in their terminology). They have shown that such material has a soft mode of shear deformation in its ground state, and the soft fluctuation is critically enhanced by random stresses. In the language of the present system, their prediction corresponds to the statement that the director fluctuation at the critical point $\lambda=\lambda_m$ is strongly enhanced by quenched disorder and satisfies $\langle|\delta\mathbf{n}(\mathbf{q})|^2\rangle\propto q^{-4}$. Nonetheless, it was not fully confirmed because of a breakdown of the harmonic approximation at the critical point, $\lambda=\lambda_m$. Also, the model
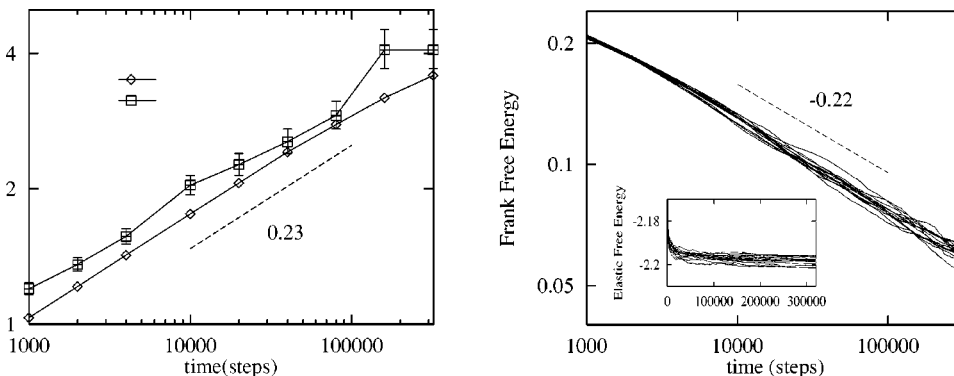

FIG. 12. Left: Evolution of the correlation length ξ and inverse peak wave number q_0^{-1}. Right: Dynamic relaxation of Frank and elastic free energies. Plotted are data from 20 individual runs.

used in [9] is quite phenomenological, and a quantitative assessment of the fluctuation enhancement is lacking. Here we extend the analysis to arbitrary values of λ, and discuss the practical possibility of finding disorder-enhanced fluctuations.

The director is decomposed into a homogeneous part and a small deviation, as

$$\mathbf{n}(\mathbf{r}) = \mathbf{e}_1 + \delta\mathbf{n}(\mathbf{r}). \tag{61}$$

Expanding the basic free energy (13) with respect to $\delta\mathbf{n}$ and $\mathbf{u}$, and then eliminating the elastic field using the mechanical equilibrium condition, we obtain an effective free energy in terms of $\delta\mathbf{n}$. An outline of the calculation is given in Appendix A. For the three-dimensional case, the result is

$$\widetilde{F}_{\mathrm{el}} = \frac{\mu\alpha}{\lambda} \int_{\mathbf{q}} \{ \tfrac{1}{2} A_1(\lambda,\hat{\mathbf{q}}) \, |\delta\mathbf{n}(\mathbf{q})|^2 + \tfrac{1}{2} A_2(\lambda,\hat{\mathbf{q}}) \, |\hat{\mathbf{q}} \cdot \delta\mathbf{n}(\mathbf{q})|^2$$

$$- R'_{ix}(\mathbf{q}) \delta n_i(-\mathbf{q}) - B_1(\lambda,\hat{\mathbf{q}}) \hat{q}_i R'_{ix}(\mathbf{q}) [\hat{\mathbf{q}} \cdot \delta\mathbf{n}(-\mathbf{q})]$$

$$- B_2(\lambda,\hat{\mathbf{q}}) [\hat{\mathbf{q}} \cdot \mathbf{R}'(\mathbf{q}) \cdot \delta\mathbf{n}(-\mathbf{q})] - B_3(\lambda,\hat{\mathbf{q}}) [\mathbf{R}'(\mathbf{q}) : \hat{\mathbf{q}}\hat{\mathbf{q}}]$$

$$\times [\hat{\mathbf{q}} \cdot \delta\mathbf{n}(-\mathbf{q})] \}, \tag{62}$$

$$A_1(\lambda,\hat{\mathbf{q}}) = \lambda^3 - 1 - \frac{3\alpha}{3+4\alpha} \frac{\lambda^6 \hat{q}_x^2}{1+(\lambda^3-1)\hat{q}_x^2}, \tag{63}$$

$A_2(\lambda,\hat{\mathbf{q}})$

$$= \frac{\dfrac{3\alpha(3+4\alpha)}{3+\alpha} \dfrac{[(3+\alpha)/(3-2\alpha)+\lambda^3]^2 \hat{q}_x^2}{3+\alpha(2+\hat{q}_x^2)} - \dfrac{3\alpha}{3-2\alpha}}{1+(\lambda^3-1)\hat{q}_x^2}, \tag{64}$$

$$B_1(\lambda,\hat{\mathbf{q}}) = \frac{1 + \dfrac{3\alpha}{3+\alpha}\left(\dfrac{3+\alpha}{3-2\alpha}+\lambda^3\right)\hat{q}_x^2}{1+(\lambda^3-1)\hat{q}_x^2}, \tag{65}$$

$$B_2(\lambda,\hat{\mathbf{q}}) = \frac{\lambda^3 \hat{q}_x}{1+(\lambda^3-1)\hat{q}_x^2}, \tag{66}$$

$$B_3(\lambda,\hat{\mathbf{q}}) = -\frac{\left(\dfrac{3+\alpha}{3-2\alpha}+\lambda^3\right)\hat{q}_x}{1+(\lambda^3-1)\hat{q}_x^2}, \tag{67}$$

$$R'_{ij}(\mathbf{q}) = \bar{\Lambda}_{ik}\bar{\Lambda}_{jl}R_{kl}(\mathbf{q}), \tag{68}$$

which is correct to the bilinear order in $\delta\mathbf{n}$ and $\mathbf{R}$ (we neglect terms independent of $\delta\mathbf{n}$).

In the absence of quenched disorder, the integrand in Eq. (62) is of the form $\tfrac{1}{2}(A_1\mathbf{I} + A_2\hat{\mathbf{q}}\hat{\mathbf{q}}):\delta\mathbf{n}(\mathbf{q})\delta\mathbf{n}(-\mathbf{q})$. It is con-

venient to introduce two unit vectors $\mathbf{e}_1 = \mathbf{q}\times\mathbf{e}_x / |\mathbf{q}\times\mathbf{e}_x|$ and $\mathbf{e}_2 = \mathbf{e}_1 \times \mathbf{e}_x$ [39], with which the integrand becomes

$$\frac{1}{2}A_1 |\mathbf{e}_1 \cdot \delta\mathbf{n}(\mathbf{q})|^2 + \tfrac{1}{2}[A_1 + A_2(1-\hat{q}_x^2)] |\mathbf{e}_2 \cdot \delta\mathbf{n}(\mathbf{q})|^2. \tag{69}$$

At $\lambda = \lambda_m$, the coefficient A_1 takes its minimum value 0 for $\mathbf{q}\|\mathbf{e}_x$, while $A_1 + A_2(1-\hat{q}_x^2)$ is minimized and vanishes both on the line $\mathbf{q}\|\mathbf{e}_x$ and in the plane $\mathbf{q}\perp\mathbf{e}_x$. These correspond to the soft modes. Similar results have been obtained by Olmsted [11] for monodomain elastomers crosslinked in the nematic phase and without external strain.

The random stresses shift the ground state to an inhomogeneous state, $\delta\mathbf{n} = \delta\mathbf{n}_R$ and $\mathbf{u} = \mathbf{u}_R$. The frozen director deviation $\delta\mathbf{n}_R$ is obtained by minimizing the total free energy $\widetilde{F}_{\mathrm{el}} + F_F$ with respect to $\delta\mathbf{n}$, as

$$\delta n_{R,i}(\mathbf{q}) = \frac{1}{A_1 + K'q^2}\left[R'_{ix}(\mathbf{q}) + B_2 \ \hat{q}_j R'_{ij}(\mathbf{q}) \right.$$

$$+ \left(B_1 - \frac{A_2(1+B_1)}{A_1+A_2+K'q^2} \right) \hat{q}_i\hat{q}_j R'_{jx}(\mathbf{q})$$

$$\left. + \left(B_3 - \frac{A_2(B_2+B_3)}{A_1+A_2+K'q^2} \right) \hat{q}_i [\hat{\mathbf{q}}\hat{\mathbf{q}}:\mathbf{R}'(\mathbf{q})] \right], \tag{70}$$

where we have introduced a scaled Frank constant,

$$K' = \frac{K\lambda}{\mu\alpha}. \tag{71}$$

At the critical point $\lambda = \lambda_m$, the quantity $A_1 + A_2$ appearing in Eq. (70) vanishes for $\mathbf{q}\perp\mathbf{e}_x$. Hence, in the long-wavelength limit $q\to 0$, we have $\delta n_R(\mathbf{q}) \propto q^{-2}$ in the soft directions $\mathbf{q}\perp\mathbf{e}_x$ and $\mathbf{q}\|\mathbf{e}_x$. This means a divergence of the real space amplitude $\langle|\delta\mathbf{n}_R(\mathbf{r})|^2\rangle$ and breakdown of the harmonic approximation, as pointed out in Ref. [9]. Severe is the divergence of the frozen elastic field $\mathbf{u}_R$, which is related to $\delta\mathbf{n}_R$ through the mechanical equilibrium condition (A2). At $\lambda = \lambda_m$, it behaves as $\langle|\mathbf{u}_R(\mathbf{q})|^2\rangle \propto q^{-6}$ in the soft directions, and $\langle|\mathbf{u}_R(\mathbf{r})|^2\rangle$ diverges. However, these divergences disappear for $\lambda > \lambda_m$, where the excess stretching acts as a stabilizing field. Now we consider this region. The condition for the harmonic approximation to be valid is $\langle|\delta\mathbf{n}_R(\mathbf{r})|^2\rangle \ll 1$, which implies $\langle|\nabla\mathbf{u}_R(\mathbf{r})|^2\rangle \ll \alpha^2$. To assess the condition by order estimate, we concentrate on the plane $\mathbf{q}\perp\mathbf{e}_x$, from which arises the most significant contribution to the real-space amplitude,

$$\langle|\delta\mathbf{n}_R(\mathbf{r})|^2\rangle = \frac{1}{(\text{system's volume})}\int_{\mathbf{q}} \langle|\delta\mathbf{n}_R(\mathbf{q})|^2\rangle. \tag{72}$$

On that plane, the strongest q dependence of $\delta n_R(\mathbf{q})$ comes from a factor $(\Delta + K'q^2)^{-1}$, where

$$\Delta = \Delta(\lambda) = [A_1(\lambda, \hat{\mathbf{q}}) + A_2(\lambda, \hat{\mathbf{q}})]|_{\hat{q}_x = 0} \qquad (73)$$

is the measure of excess stretching. Note that $\Delta \propto \lambda - \lambda_m$ for $\lambda - \lambda_m \ll 1$. A saddle-point approximation around the plane yields

$$\langle |\delta \mathbf{n}_R(\mathbf{r})|^2 \rangle \sim \int \frac{\beta^2 \xi_R^3 q^2 dq}{(\Delta + K' q^2)^{3/2}}$$

$$\times \begin{cases} \sim \dfrac{\beta^2 \xi_R^3}{K'^{3/2}} \ln\left(\dfrac{K' q_{\max}^2}{\Delta}\right) & (\Delta \ll K' q_{\max}^2), \\[3mm] \sim \dfrac{\beta^2 \xi_R^3}{K'^{3/2}} \left(\dfrac{K' q_{\max}^2}{\Delta}\right)^{3/2} & (\Delta \gg K' q_{\max}^2), \end{cases}$$

$$(74)$$

where $q_{\max}$ is the upper cutoff wave number. We may roughly identify $2\pi/q_{\max}$ with the network mesh size, $l \sim (k_B T/\mu)^{1/3}$. Using typical experimental values $\mu = 10^5$ J/m³, $K = 10^{-11}$ J/m, $\alpha = 1.0$, and $T = 300$ K, we have $\sqrt{K'} = 10$ nm and $K' q_{\max}^2 \sim 1$. For $\Delta \lesssim K' q_{\max}^2$ and except in the close vicinity of the criticality, $\Delta = 0$, the amplitude only weakly depends on the elongation ratio. In this region, the harmonic approximation is valid if and only if

$$\frac{\beta^2 \xi_R^3}{K'^{3/2}} \ll 1, \qquad (75)$$

which is satisfied when we set $\xi_R \sim 10^2$ nm and $\beta \sim 0.01$ as a trial.

The director exhibits a thermal fluctuation around the inhomogeneous ground state. Its amplitude is not affected by the quenched randomness, at least within the harmonic calculation. The total fluctuation amplitude is given by

$$P^{(a)}(\mathbf{q}) = \langle |\mathbf{e}_a \cdot \delta \mathbf{n}(\mathbf{q})|^2 \rangle = P_T^{(a)}(\mathbf{q}) + P_R^{(a)}(\mathbf{q}), \qquad (76)$$

$$P_T^{(a)}(\mathbf{q}) = \frac{k_B T \lambda}{\mu \alpha} \frac{1}{A_1 + \delta_{a2}(1 - \hat{q}_x^2) A_2 + K' q^2}, \qquad (77)$$

$$P_R^{(a)}(\mathbf{q}) = \langle |\mathbf{e}_a \cdot \delta \mathbf{n}_R(\mathbf{q})|^2 \rangle, \qquad (78)$$

where $a = 1, 2$ and $P_T^{(a)}$ and $P_R^{(a)}$ are the thermal and frozen contributions, respectively. Let us compare the two contributions. To be explicit, we compare $P_T^{(2)}(\mathbf{q})$ and $P_R^{(2)}(\mathbf{q})$ on the plane $\mathbf{q} \perp \mathbf{e}_x$. There the ratio $P_R^{(2)}/P_T^{(2)}$ is controlled by a factor of the form $\Delta_c/(\Delta + K' q^2)$, where

$$\Delta_c = \frac{\mu \alpha \beta^2 \xi_R^3}{k_B T} \qquad (79)$$

defines a crossover point. In the region $\Delta \lesssim \Delta_c$, the disorder part of the fluctuation dominates the thermal part at long wavelengths. We estimate $\Delta_c \sim 10^{-3}$ using the above-mentioned values, for which the crossover length $\sqrt{K'/\Delta_c}$
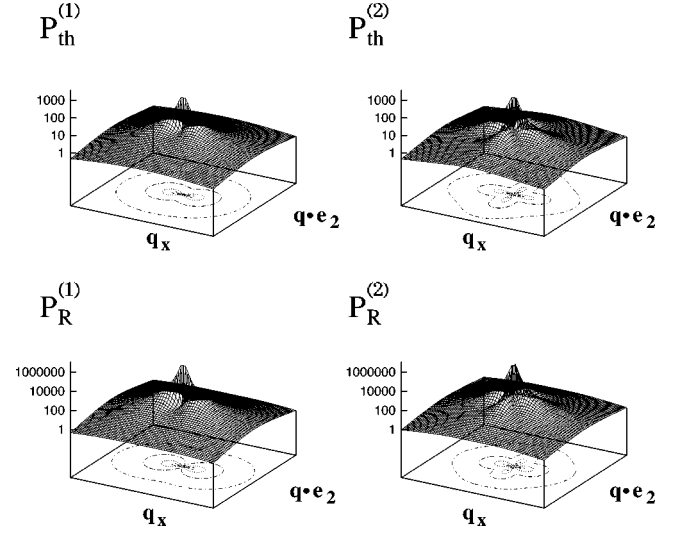

FIG. 13. Square amplitudes of director fluctuation (in arbitrary unit). $P_R^{(1)}$ and $P_R^{(2)}$ are multiplied by a common prefactor. Shown is the region $-30 < K'^{1/2} q_x < 30$ and $-30 < K'^{1/2} \mathbf{q} \cdot \mathbf{e}_2 < 30$. Note the strong $|q|$ dependence of the disorder contribution.

$\sim 10^2 - 10^3$ nm is around or below the wavelength of visible light. The amplitudes for $\alpha = 0.2$ and $\lambda/\lambda_m = 1.001$ are plotted in Fig. 13. We see that the anisotropy of the scattering pattern is not much affected by the quenched disorder.

The director fluctuation amplitudes are closely related to polarized light scattering intensity [39]. By comparing experimental results to the above calculation, we may extract information on the network heterogeneity. In particular, if the macroscopic orientation is not saturated in the monodomain state, it means the presence of large-scale quenched strains that do not meet the condition (75). For instance, in an optical study of a swollen monodomain gel by Chang *et al.* [50], speckles on the few-micrometer scale are observed, which is attributed to heterogeneities as we consider here. We hope that the scattering intensity will be measured as a function of applied strain. Another origin of large-scale heterogeneity will be discussed in Sec. V.

B. Effect of fractal heterogeneity

Up to now we assumed that the network heterogeneity has a single characteristic size ξ_R and the random stresses lack correlation beyond this length. This is a good approximation for densely crosslinked elastomers and gels that are far beyond the gel point. However, gels at or close to the gel point are better characterized by a fractal network structure, as deduced from the percolation theory [33,51,52] and as experimentally confirmed [53,54]. Since the statistics of the heterogeneity strongly affect the long-wavelength behavior of the structure factor, it is worthwhile to generalize the results of the previous sections to include a class of fractal heterogeneity. The random stresses are now assumed to obey

$$\langle R_{ij}(\mathbf{q}) R_{kl}(-\mathbf{q}) \rangle = \xi_R^{2d - d_F} q^{d - d_F}$$

$$\times \left[\beta^2 \left(\delta_{ik} \delta_{jl} + \delta_{il} \delta_{jk} - \frac{2}{d} \delta_{ij} \delta_{kl} \right) \right.$$

$$\left. + \beta'^2 \delta_{ij} \delta_{kl} \right], \qquad (80)$$

which reduces to Eq. (9) when the fractal dimension d_F is equal to the spatial dimension d. The length ξ_R is now interpreted as the lower cutoff size below which the simple asymptotic behavior (80) no longer holds. A straightforward generalization of the Imry-Ma argument gives the condition for breaking of the long-range order,

$$d < \frac{4 + 2d_F}{3}, \tag{81}$$

which, for the physical dimension $d=3$, is met only if $d_F > 2.5$.

The soft fluctuation at the polydomain-monodomain threshold has an amplitude $\langle |\delta\mathbf{n}_R(\mathbf{q})|^2 \rangle \propto q^{-2(d_F - d + 2)}$. If $d_F < d$, the real-space amplitude $\langle |\delta\mathbf{n}_R(\mathbf{r})|^2 \rangle$ converges and its strain dependence is controlled by a factor $1 - (\Delta/K' q_{\max}^2)^{d - d_F}$ for $\Delta \ll K' q_{\max}^2$.

V. THE CASE OF ANISOTROPIC CROSSLINKING: STRONG DISORDER REGIME

The almost completely soft mechanical response as we have described in Sec. III is not always observed in experiments. In fact, direct evidence of a vanishingly small stress is rather scarce [15,17]. In many other cases, a finite and sizable plateau stress is found in the PM transition region of the strain-stress curve. An existing theory [22] for such ''nonsoft'' response assumes that an external strain makes the elastic free energy localized in thin domain walls. The theory estimates the plateau stress to be of $O(\alpha)$ in the presence of weak quenched randomness. However, from the results of the previous sections, we know that weak disorder allows nonlocal domain reorganization and the coupling free energy $-\alpha\mathbf{Q}:\nabla\mathbf{u}$ makes a nonpositive contribution to the stress. Hence we argue that the observed nonsoft response is caused by some *strong disorder effect*, which is presumably due to large-scale frozen heterogeneity. In this section, we study the mechanical property and associated spatial structure in the strong disorder regime.

As a possible realization of strong disorder, we consider the case of anisotropic crosslinking. Melts of nematic polymers often exhibit long-lived polydomain textures after a quench from the isotropic phase [55–57]. The size of the domains is macroscopic and typically of micron order. When such a melt is crosslinked, its nonuniform orientation is imprinted into the network. We denote the initial configuration by $\mathbf{Q}_0(\mathbf{r})$. The extended affine-deformation theory prescribes the elastic free energy,

$$F_{\mathrm{el}} = \frac{\mu}{2} \int d\mathbf{r} \ \mathrm{Tr}[(\mathbf{I} + \alpha_0\mathbf{Q}_0)\cdot\Lambda^T\cdot(\mathbf{I} - \alpha\mathbf{Q})\cdot\Lambda - \mathbf{I}], \tag{82}$$

where α_0 is expressed in terms of the parameters used in [12] as

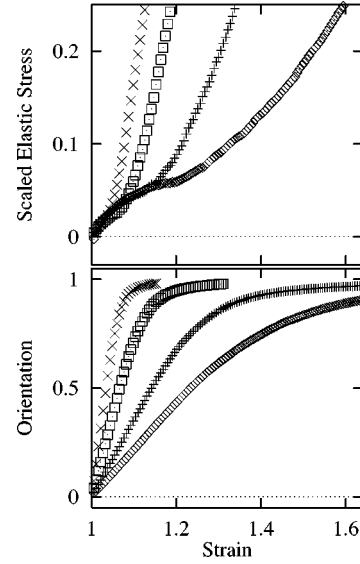$$\alpha_0 = \frac{\ell_\parallel - \ell_\perp}{(1/d)\ell_\parallel + (1 - 1/d)\ell_\perp}, \tag{83}$$

FIG. 14. Strain-stress and strain-orientation curves for the case of anisotropic crosslinking. Plotted for cases $\alpha = 0.2$, 0.4, 0.8, and 1.2 from the left to right, with $\mu\alpha^2 = 16$ in common.

or equivalently, $\alpha_0 = \alpha/[1 - (1 - 2/d)\alpha]$. Note that the above free energy is obtained by just formally replacing $\mathbf{R}$ with $\alpha_0\mathbf{Q}_0$ in the free energy (13). Thus, the initial texture field $\mathbf{Q}_0$ provides a source of quenched disorder. Effective disorder strength that corresponds to Eq. (31) can be defined by

$$D = \frac{\mu\alpha\alpha_0}{K} \xi_0^2, \tag{84}$$

where ξ_0 is the correlation length of the initial texture. If we set $\xi_0 = 1$ μm and $\alpha = 0.1$, we have a very large number $D \sim (\xi_0/\xi_c)^2 = 10^3$–$10^5$. Since the orientational order is predominantly affected by this strong disorder, we do not take into account other mesoscopic sources of quenched stresses, which is legitimate as a first approximation.

We have simulated the PM transition in the following way. To generate the initial configuration, we mimicked the phase-ordering kinetics of nematic polymer solutions by numerically solving the equation

$$\frac{\partial\mathbf{n}}{\partial t} = -\Gamma_n (\mathbf{I} - \mathbf{nn}) \cdot \frac{\delta F_F}{\delta\mathbf{n}}. \tag{85}$$

Taking a sitewise-random director configuration as the initial condition, we integrated Eq. (85) over 50 time steps (with $\Gamma_n = 0.2$ and $\Delta t = 1$) to generate $\mathbf{Q}_0(\mathbf{r})$. After crosslinking the system by adding F_{el} to the free energy and setting $\lambda = 1$ and $\mathbf{u} = 0$, we integrated Eqs. (59) and (60) for 1×10^4 time steps to equilibrate the system. The mechanical response was studied in just the same way as described in Sec. III.

Figure 14 shows the strain-stress and strain-orientation curves for $\alpha = 0.2$, 0.4, 0.8, and 1.2. The strain-stress curve bends at a value of λ where the director is still far from aligned. For $\alpha \geq 0.8$, the gradient of the strain-stress curve has a nonmonotonic dependence on the strain, and is smallest at an intermediate value of λ. This is in qualitative agree-
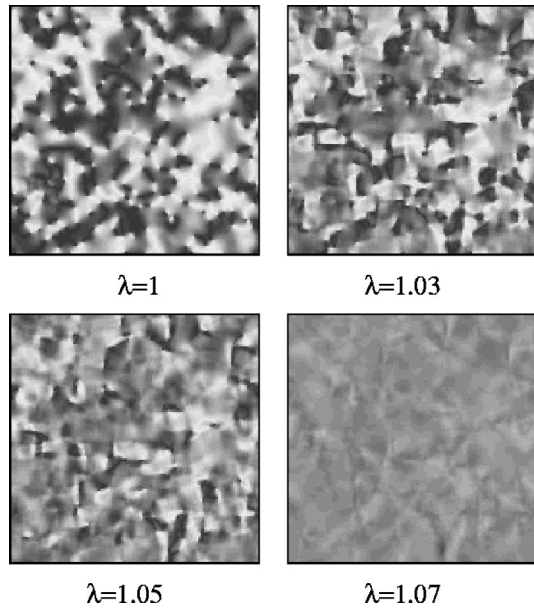
FIG. 15. Snapshots of the field $Q_{xy}(\mathbf{r})$ for the case of anisotropic crosslinking. The director texture of the nematic liquid just before crosslinking is retained at $\lambda = 1$.

ment with the observed plateau behavior, although the plateau region is not clearly distinguishable from other regions. The strain-orientation curve shows only a gradual crossover to the monodomain state, especially for larger values of α. The slope of the scaled elastic stress $\mu^{-1}\sigma_{\mathrm{macro}}$ is roughly independent of α in the vicinity of the point $\lambda = 1$.

Evolution of the director texture during the PM transition is shown in Fig. 15, and the distribution of the elastic free energy is shown in Fig. 16. At $\lambda = 1$, the director texture is almost the same as that just before crosslinking, or $\mathbf{Q}(\mathbf{r}) = \mathbf{Q}_0(\mathbf{r})$. This is reflected in the extremely homogeneous free-energy distribution. External strain strongly dehomogenizes the distribution, and the peak is continuously broadened as we increase λ toward the monodomain region.

VI. DISCUSSION AND SUMMARY

We have studied polydomain nematic networks from two aspects, namely, (i) breaking of long-range orientational order by frozen internal stresses and (ii) a nonlocal interdomain
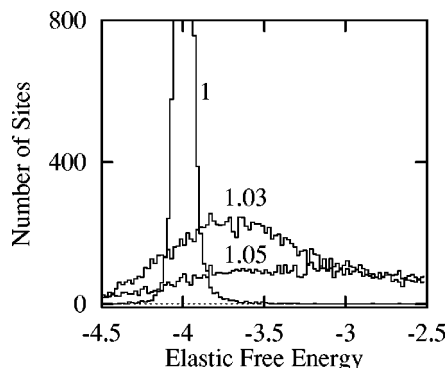

FIG. 16. Histogram of the elastic free energy contained in a site. Cases $\lambda = 1$, 1.03, and 1.05 are shown. The peak for $\lambda = 1$ is out of the window and counts more than 3000 sites.

interaction arising from strain-orientation coupling. The mechanical response is controlled by the latter if the quenched disorder is of moderate strength (or if $D \lesssim 1$). In this case, the proper elastic interaction reorganizes the polydomain structure so that local elongation along the director is achieved everywhere in the system. The resulting structure contains the checkered correlation pattern on various scales, which produces the ''four-leaf clover'' pattern in the depolarized scattering intensity. Upon stretching, the director and the local strain axis coincidently rotate toward the direction of macroscopic extension, and thus the elastic free energy keeps almost constant until a complete alignment is attained. The change in elastic free energy accompanying the PM transition is analytically estimated to be of $O(\alpha^3)$. This result does not depend on a specific model of nonlinear elasticity. In fact, we obtained it by harmonic expansion of the elastic free energy, which is unique from symmetry [7]. Numerical simulation reveals a more complete softness, and we find essentially no α dependence of the average macroscopic stress (47). We cannot exclude the theoretical possibility that the PM transition is exactly soft in the weak disorder limit. We may say that there are mechanical *quasi-Goldstone modes*, which are distinguished from the genuine Goldstone modes of fluid nematic liquid crystals in that there is a strongly anisotropic correlation even in the absence of external field and that the quenched disorder selects a characteristic length scale.

We have discussed two sources of quenched disorder. One is the random stress due to residual heterogeneous strains at the moment of crosslinking, considered ubiquitous in rubbery networks. The anisotropic (shear) part of random stresses acts on the orientational order, both locally and nonlocally. The macroscopic domain size observed in experiments can be explained if there are frozen heterogeneities of a reasonably small magnitude (e.g., 1% in strain) and a size somewhat larger than that of individual network meshes (e.g., 10^2 nm).

A different viewpoint was taken in previous theories [20–22], where a random molecular field operating at crosslinks was assumed to be the source of disorder. The random field hypothesized there has a small correlation length roughly equal to the distance l between crosslinks. The ratio ξ/l is a large number ($\sim 10^3$), which means a weak effective disorder.

Currently we know of no firm experimental indication of the disorder strength. A possible method of its estimate is to observe director fluctuation in the monodomain state. We have calculated thermal and disorder contributions to the fluctuation amplitude, which is proportional to the polarized light scattering intensity. The intensity diminishes as we stretch the network, and there is a region of macroscopic strain λ where the disorder contribution dominates over the thermal one. The width of the region and the absolute value of the intensity should tell us the order of the disorder strength. The thermal and quenched contributions could be separately analyzed by use of dynamical light scattering (DLS). Indeed, DLS has been successfully used to decompose the two kinds of density fluctuation in gels [2]. It is hoped that a similar method will be developed for orientation fluctuation in the present system.

By crosslinking the network in the nematic phase and in

the course of phase ordering, we obtain another kind of quenched stress. The polydomain texture of the liquid-crystalline polymer melt is almost completely frozen by crosslinking, if its characteristic size is larger than ξ_c. The memory of the initial macroscopic texture makes the mechanical response nonsoft. Spatial distribution of the elastic free energy is strongly dehomogenized by applied strain, in contrast to the case of isotropic crosslinking.

The influence of crosslinking conditions has seldom been discussed in previous studies of the PM transition, except for a few experimental papers [14,17]. Küpfer and Finkelmann [14] studied both isotropic and anisotropic crosslinkings under external stress of various magnitudes. Figure 8 in the reference shows that polydomain networks crosslinked in the nematic phase are harder than those prepared in the isotropic phase. Another example of soft and nonsoft PM transitions is given in Ref. [17], where it is stated that some of their samples were prepared above the isotropic-nematic transition temperature of the melt, while the others are crosslinked below it. Unfortunately, they do not explicitly state the crosslinking condition for each stress-strain curve. We hope there will be further effort in this direction in the future, especially to find more evidence of vanishing macroscopic stress.

A remark should be made in relation to this. We have assumed that the quenched heterogeneities have mesoscopic sizes in the case of isotropic crosslinking. However, if the network is crosslinked in poor solvents or near the spinodal line, the heterogeneities can be macroscopic and cause strong effective disorder. Therefore, the mechanical response should be discussed in terms of the size of the heterogeneity, not only on the phase where the gel is fabricated. Another problem in interpretation of strain-stress data arises from the slowness of dynamical relaxation. A recent dynamic measurement by Clarke and Terentjev [18] strongly suggests that the stress level will be substantially lowered in the final equilibrium state, which is not reachable on a practical time scale. It might be possible that a soft equilibrium PM transition is masked behind a stress plateau of a sizable height, which was reported in earlier studies [13,14].

We have studied dynamical relaxation after a quench from the isotropic phase. The structure factor develops a peak at a finite wave number, which goes to zero as the true equilibrium is approached. Both the inverse peak wave number and the correlation length show a power-law type growth in an intermediate stage, while the elastic free energy is almost completely minimized in an early regime of the coarsening process.

Some of the experimentally observed features of the ''four-leaf clover'' scattering pattern have been reproduced in the present work. First, we propose that the finiteness of the observed peak wave number is explained by the slow relaxation. The experimental peak wave number does not change during the PM transition [16]. Together with our simulation result, it suggests that the coarsening is very slow and does not occur in the time scale of observation. Further experimental study of structural relaxation in conjunction with stress relaxation would be informative to check this point. Second, the peak intensity increases and then decreases as we stretch the gel. Qualitatively, the same monotonic behavior is reported in the experiment. The initial in-

crease is due to a sharpening of the peak, which is partially understood by the fact that the director fluctuation at $\lambda = \lambda_m$ is soft only on a plane and a line in the $\mathbf{q}$ space.

We close by listing some open questions. (i) We did not answer whether the long-range order is destroyed by an *arbitrarily* weak disorder under *no external stress* or, equivalently, when the average strain λ is not externally constrained. A shift of the ground state from monodomain ($\lambda = \lambda_m$) to polydomain ($\lambda = 1$) states should occur, either gradually or abruptly, as we increase the disorder strength from zero. Probably this problem is not of practical importance because of a small but finite hysteresis and the slow dynamics. (ii) Stretching-induced anisotropy of the depolarized scattering pattern as we numerically find is contrary to the experimental observation. We may suggest an effect of spatial dimensionality. In three dimensions there are three Frank constants, whose relative strengths may affect the anisotropy. Experimental investigation of 3D domain structure would be informative. (iii) Much remains to be done for understanding dynamical relaxation to the final equilibrium state. In the theoretical part, the origin of the apparent power law is yet unknown. Dynamic equations for dry elastomers are to be constructed, taking intranetwork friction into account. In the numerical part, late stages of the relaxation process are left unexplored. Stress relaxation for strong quenched disorder and after stretching should be addressed to make a comparison to experiment. As these necessitate extensive computation, we leave them for future work.

APPENDIX A: EFFECTIVE FREE ENERGY IN THE MONODOMAIN STATE

Here we sketch the derivation of Eq. (62). Substituting Eqs. (17), (18), and (19) into Eq. (13), we have

$$F_{\text{el}} = \frac{\mu}{2} \int d\mathbf{r} [C_{ij} L_{ij} + 2 C_{ik} L_{jk} (\partial_i u_j) + \bar{C}_{ij} \bar{L}_{kl} (\partial_i u_k)(\partial_j u_l) + \kappa (\partial_i u_i)^2], \tag{A1}$$

where $C_{ij} = (\delta_{kl} + R_{kl}) \bar{\Lambda}_{ik} \bar{\Lambda}_{jl}$ and $L_{ij} = \delta_{ij} - \alpha Q_{ij} = (1 + \alpha/3) \delta_{ij} - \alpha n_i n_j$. In the third term of the integrand we have replaced C_{ij} and L_{ij} with their spatial averages as the deviations will contribute only to higher-order terms in the effective free energy. The last term is added by hand to temporarily relax the incompressibility condition (23), which is recovered by taking the limit $\kappa \to \infty$ afterwards. The condition of mechanical equilibrium (22) can be written as

$$\partial_i (C_{ik} L_{jl}) + \bar{C}_{ij} \bar{L}_{kl} \partial_i \partial_j u_k + \kappa \partial_i \partial_j u_j = 0. \tag{A2}$$

Taking the incompressible limit $\kappa \to \infty$, we have

$$\mathbf{u}(\mathbf{q}) = \frac{1}{\mathbf{C}:\mathbf{qq}} \left[\mathbf{L}^{-1} \cdot \mathbf{g}(\mathbf{q}) - \frac{\mathbf{L}^{-1} \cdot \mathbf{q}}{\mathbf{L}^{-1}:\mathbf{qq}} \left[\mathbf{q} \cdot \mathbf{L}^{-1} \cdot \mathbf{g}(\mathbf{q}) \right] \right],$$

$$(A3)$$

where $\mathbf{g}$ is an auxiliary variable defined by

$$g_i(\mathbf{r}) = \partial_j(C_{jk}L_{ik}). \qquad (A4)$$

Substituting Eq. (A3) into Eq. (A1), we obtain an effective free energy,

$$\tilde{F}_{\mathrm{el}} = \frac{\mu}{2} \int d\mathbf{r} \mathbf{C}:\mathbf{L} + \frac{\mu}{2} \int_{\mathbf{q}} \frac{1}{\overline{\mathbf{C}}:\hat{\mathbf{q}}\hat{\mathbf{q}}} \left[\frac{1}{\overline{\mathbf{L}}^{-1}:\hat{\mathbf{q}}\hat{\mathbf{q}}} \hat{\mathbf{q}} \cdot \overline{\mathbf{L}}^{-1} \cdot \mathbf{g}(\mathbf{q}) \right]^2$$

$$- \mathbf{g}(\mathbf{q}) \cdot \overline{\mathbf{L}}^{-1} \cdot \mathbf{g}(-\mathbf{q}) \bigg], \qquad (A5)$$

We arrive at Eq. (62) by setting Eq. (17) into C_{ij}, Eq. (61) into L_{ij}, and the resulting expressions into Eqs. (A4) and (A5).

---

[1] K. Dušek and W. Prins, Adv. Polym. Sci. **6**, 1 (1969).

[2] For a recent review, see M. Shibayama, Macromol. Chem. Phys. **199**, 1 (1998).

[3] E. Mendes, P. Lindner, M. Buzier, F. Boue, and J. Bastide, Phys. Rev. Lett. **66**, 1595 (1991).

[4] J. Bastide, L. Leibler, and J. Prost, Macromolecules **23**, 1821 (1990).

[5] A. Onuki, J. Phys. II **2**, 45 (1992).

[6] For a review, see J. Bastide and S. J. Candau, in *Physical Propertires of Polmeric Gels*, edited by J. P. Cohen Addad (Wiley, New York, 1996), Chap. 5.

[7] P. G. de Gennes, C. R. Seances Acad. Sci., Ser. B **281**, 101 (1975).

[8] M. Warner, K. P. Gelling, and T. A. Vilgis, J. Chem. Phys. **88**, 4008 (1988).

[9] L. Golubović and T. C. Lubensky, Phys. Rev. Lett. **63**, 1082 (1989).

[10] M. Warner, P. Bladon, and E. M. Terentjev, J. Phys. II **4**, 93 (1994).

[11] P. D. Olmsted, J. Phys. II **4**, 2215 (1994).

[12] For a review, see M. Warner and E. M. Terentjev, Prog. Polym. Sci. **21**, 853 (1996);, and references therein.

[13] J. Schätzle, W. Kaufhold, and H. Finkelmann, Macromol. Chem. Phys. **190**, 3269 (1989).

[14] J. Küpfer and H. Finkelmann, Macromol. Chem. Phys. **195**, 1353 (1994).

[15] G. H. F. Bergmann, H. Finkelmann, V. Percec, and M. Zhao, Macromol. Rapid Commun. **18**, 353 (1997).

[16] S. M. Clarke, E. M. Terentjev, I. Kundler, and H. Finkelmann, Macromolecules **31**, 4862 (1998).

[17] E. R. Zubarev, R. V. Talroze, T. I. Yuranova, N. A. Plate, and H. Finkelmann, Macromolecules **31**, 3566 (1998). They obtained both soft and nonsoft PM transitions, as seen in their Figs. 7 and 6, respectively.

[18] S. M. Clarke and E. M. Terentjev, Phys. Rev. Lett. **81**, 4436 (1998).

[19] Early experiments on polydomain elastomers are reviewed in H. R. Brand and H. Finkelmann, in *Handbook of Liquid Crystals*, edited by D. Demus *et al.* (Wiley-VCH, New York, 1998), Vol. 3, Chapter V.

[20] A. ten Bosch and L. Varichon, Macromol. Theory Simul. **3**, 533 (1994).

[21] S. M. Clarke, E. Nishikawa, H. Finkelmann, and E. M. Terentjev, Macromol. Chem. Phys. **198**, 3485 (1997).

[22] S. V. Fridrikh and E. M. Terentjev, Phys. Rev. Lett. **79**, 4661 (1997); Phys. Rev. E **60**, 1847 (1999).

[23] L. D. Landau and E. M. Lifshitz, *Theory of Elasticity*, 3rd ed. (Pergamon, Oxford, 1986).

[24] K. H. Lau and W. Kohn, Surf. Sci. **65**, 607 (1977).

[25] V. I. Marchenko and A. Y. Parshin, Zh. Éksp. Teor. Fiz. **79**, 257 (1980) [Sov. Phys. JETP **52**, 129 (1980)].

[26] J. W. Cahn, Acta Metall. **9**, 795 (1961).

[27] A. Onuki, J. Phys. Soc. Jpn. **58**, 3065 (1989); , *ibid.* **58**, 3069 (1989).

[28] T. Tanaka, S. -T. Sun, Y. Hirokawa, S. Katayama, J. Kucera, Y. Hirose, and T. Amiya, Nature (London) **325**, 796 (1987).

[29] For a review, see A. Onuki, Adv. Polym. Sci. **109**, 63 (1993), and references therein.

[30] M. Goulian, R. Bruinsma, and P. Pincus, Europhys. Lett. **22**, 145 (1993).

[31] N. Uchida and A. Onuki, Europhys. Lett. **45**, 341 (1999).

[32] N. Uchida, Phys. Rev. E **60**, R13 (1999).

[33] P. G. de Gennes, *Scaling Concepts in Polymer Physics* (Cornell University Press, NY, Ithaca, 1980).

[34] S. Alexander, J. Phys. (France) **45**, 1939 (1984).

[35] For a work in this direction, see S. Panyukov and Y. Rabin, Macromolecules **29**, 7960 (1996).

[36] P. J. Flory, *Principles of Polymer Chemistry* (Cornell University Press, Ithaca, NY, 1953).

[37] A. E. H. Love, *A Treatise on the Mathematical Theory of Elasticity*, 4th ed. (Dover, New York, 1944).

[38] P. J. Flory, Trans. Faraday Soc. **56**, 722 (1960). This paper derives the free energy of a network crosslinked in two stages. If we assume a two-stage crosslinking with null crosslinks introduced in the first stage and succeeding deformation **R** before the second one, we obtain Eq. (6).

[39] P. G. de Gennes and J. Prost, *The Physics of Liquid Crystals*, 2nd ed. (Oxford University Press, Oxford, 1993).

[40] Y. Imry and S. -K. Ma, Phys. Rev. Lett. **35**, 1399 (1975).

[41] The elastic stress tensor σ_{ij} for the full nonlinear model (13) is computed through the change in free energy for an infinitesimal displacement $\delta\mathbf{u}$,

$$\delta F_{\mathrm{el}} = \int d\mathbf{r}\, \sigma_{ij} \partial_i \delta u_j. \qquad (A6)$$

Using the relation $\delta\Lambda_{ij} = \Lambda_{kj}\partial_k u_i$, we obtain the stress tensor as

$$\sigma_{ij} = \mu(\delta_{ik} + R_{ik})(\delta_{lm} - \alpha Q_{lm})\Lambda_{jl}\Lambda_{km}. \qquad (A7)$$

Expanding it with respect to $\nabla\mathbf{u}$ and subtracting a hydrostatic term proportional to δ_{ij}, we arrice at Eq. (48). The case of a clean nematic gel is found in P. D. Olmsted and S. T. Milner,

Macromolecules **27**, 6648 (1994).

[42] W. H. Press, A. A. Teukolsky, W. T. Vetterling, and B. P. Flannery, *Numerical Recipes in C*, 2nd ed. (Cambridge University Press, Cambridge, 1992).

[43] B. Dieny and B. Barbara, Phys. Rev. B **41**, 11 549 (1990).

[44] M. J. P. Gingras and D. A. Huse, Phys. Rev. B **53**, 15 193 (1996).

[45] Y. -K. Yu, P. L. Taylor, and E. M. Terentjev, Phys. Rev. Lett. **81**, 128 (1998).

[46] To be strict, flow of the solvent should be taken into account. The relation $\partial\mathbf{u}/\partial t \propto -\delta F/\delta\mathbf{u}$ holds in the limit where the solvent viscosity is infinitely large. A similar simplified dynamic equation has been used, for instance, for describing swelling dynamics in T. Hwa and M. Karder, Phys. Rev. Lett. **61**, 106 (1988).

[47] J. L. Harden, H. Pleiner, and P. A. Pincus, J. Chem. Phys. **94**, 5208 (1990).

[48] A. J. Bray, Adv. Phys. **43**, 357 (1994).

[49] Even in the absence of quenched disorder, the simple scaling result $\epsilon' = 2\epsilon$ is apparently broken due to a strong finite-size effect in 2D. See [48] and M. Zapotocky, P. M. Goldbart, and N. Goldenfeld, Phys. Rev. E **51**, 1216 (1995).

[50] C. -C. Chang, L. -C. Chien, and R. B. Meyer, Phys. Rev. E **56**, 595 (1997).

[51] D. Stauffer, A. Coniglio, and M. Adam, Adv. Polym. Sci. **44**, 104 (1982).

[52] H. J. Hermann, Phys. Rep. **136**, 153 (1986).

[53] M. Adam, D. Lairez, F. Boué, J. P. Busnel, D. Durand, and T. Nicolai, Phys. Rev. Lett. **67**, 3456 (1991).

[54] J. E. Martin, D. Adolf, and J. P. Wilcoxon, Phys. Rev. Lett. **61**, 2620 (1988).

[55] T. Takebe, T. Hashimoto, B. Ernst, P. Navard, and R. S. Stein, J. Chem. Phys. **92**, 1386 (1990).

[56] F. Elias, S. M. Clarke, R. Peck, and E. M. Terentjev, Europhys. Lett. **47**, 442 (1999).

[57] M. Doi and S. F. Edwards, *The Theory of Polymer Dynamics* (Oxford University Press, Oxford, 1986), Sec. 10.6 and references therein.